Chapter 2

Structural and Dynamic Properties of Group 5 *ansa*-Metallocene Tetrahydroborate Complexes

2.1 Introduction to Chapter 2

This chapter describes the preparation of new Group 5 *ansa*-metallocenes. In particular it is concerned with the relationship between the structural and dynamic properties of the tetrahydroborate derivatives. A systematic study of the effect of varying the bridging unit of the *ansa*-metallocene on bridge-terminal hydrogen exchange in the BH_4 ligand has been carried out. Each new compound is described separately in **Section 2.3.** A comparison of the structural, dynamic and electronic properties of these new compounds is described in **Section 2.5.** A density functional study of the mechanism of bridge-terminal hydrogen exchange is presented in **Section 2.6.**

2.2 Hydrogen Exchange in Metallocene Tetrahydroborate Complexes

The chemistry of the d- and f-block metals bearing the tetrahydroborate ligand BH_4 has been extensively studied.[1] Three modes of bonding of the tetrahydroborate unit have been reported (**Figure 2.1**). The relatively uncommon monodentate ligation has been reported for the compounds $[Cu(BH_4)(PMePH_2)_2]$,[2] $[Fe(BH_4)H(dmpe)_2]$[3] and the 15 electron complex $[V(BH_4)_2(dmpe)_2]$.[4] The tridentate mode has been structurally characterised in a small number of complexes such as $[Al(BH_4)_3]$[5] and $[M(BH_4)_4]$ (M = Zr or Hf).[6]

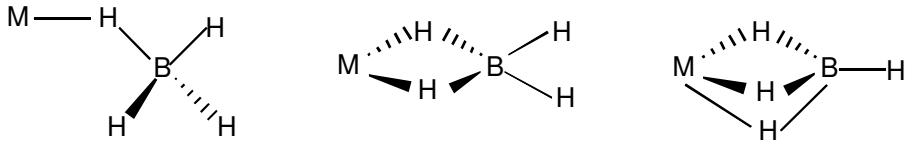

Figure 2.1 Various bonding modes of tetrahydroborate complexes of d- and f-block metals

By far the most common mode of bonding is bidentate $(\mu\text{-}H)_2BH_2$ ligation. This mode is extensively found for metallocene tetrahydroborate complexes of the type $[M(\eta\text{–}C_5H_5)_2(\eta^2\text{–}BH_4)]$ (M = Ti, V, Nb)[7-9] and the *ansa*-niobocene compound $[Nb\{(\eta\text{–}C_5H_4)CMe_2(\eta\text{–}C_5H_4)\}(\eta^2\text{–}BH_4)]$.[10] Neutron diffraction studies have shown that

the compound $[Hf(\eta\text{–}C_5H_4Me)_2(\eta^2\text{–}BH_4)_2]$ possesses two bidentate tetrahydroborate ligands.[11]

In most cases tetrahydroborate complexes are fluxional on the ^1H NMR time scale. In tridentate species the exchange pathway is proposed to proceed *via* reversible dissociation of a bridging hydrogen to form a bidentate intermediate.[12] Rapid rotation about the three-fold axis of the ligand accounts for exchange of the bridging hydrogens in this model.

Exchange between the bridging and terminal hydrogens of the bidentate BH_4 unit is also facile. In certain cases such as $[M(\eta\text{–}C_5H_5)_2(\eta^2\text{–}BH_4)]$ (M = Nb, V) the free energy barrier to bridge-terminal hydrogen exchange $\Delta G^{\ddagger}$ is sufficiently large that the fluxional behaviour becomes slow on the ^1H NMR time scale.[8] The mechanism of exchange in bidentate tetrahydroborate complexes has prompted considerable debate. Early mechanistic studies favoured a dissociative mechanism involving a unidentate BH_4 intermediate (**Figure 2.2**).[8]

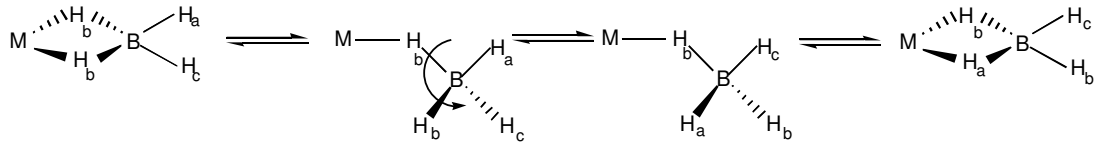

Figure 2.2 Proposed dissociative mechanism *via* a unidentate BH_4 intermediate for exchange of bridging and terminal hydrogens.

A detailed 2D exchange (EXSY) ^1H NMR study of $[Ta(\eta\text{–}C_5H_5)(\eta\text{–}C_5Me_5)(\eta^2\text{–}BH_4)]$ showed that there is negligible direct exchange between the terminal hydrogens.[13] A mechanism involving η^5-η^3 ring shift of one of the cyclopentadienyl rings upon coordination of a terminal hydrogen to the metal centre in an $\eta^3\text{–}BH_4$ intermediate has been proposed (**Figure 2.3**). Either of these steps may be rate-limiting. Rotation of the coordinated η^3-BH_4 unit would result in the exchange of bridging and terminal hydrogens.

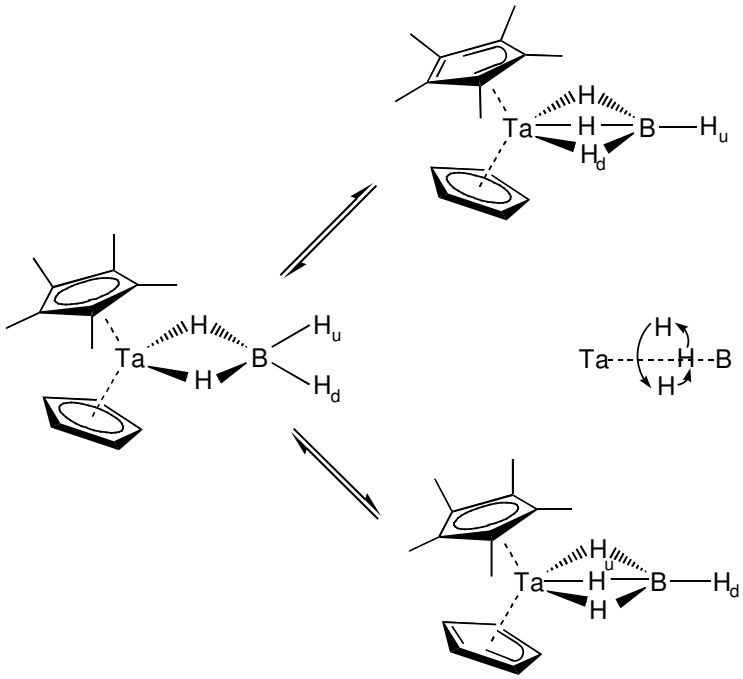

Figure 2.3 Proposed associative mechanism *via* a tridentate intermediate for exchange of bridging and terminal hydrogens in $[Ta(\eta-C_5Me_5)(\eta-C_5H_5)(\eta^2-BH_4)]$.

In the light of the observations of Green and Wong it was decided to explore the effect of the presence of an *ansa*-bridge on the exchange processes in Group 5 metallocene tetrahydroborate complexes. For instance, for a rate-limiting step involving an η^5-η^3 ring shift a lower energetic barrier to hydrogen exchange would be expected when the strain imparted by the bridging unit is greatest. There are a small number of Group 5 *ansa*-metallocenes described in the literature,[14-20] while the only known *ansa*-metallocene tetrahydroborate complex $[Nb\{(\eta-C_5H_4)CMe_2(\eta-C_5H_4)\}(\eta^2-BH_4)]$ was prepared previously in this laboratory.[10] However, no quantitative information regarding the free energy barrier to bridge-terminal hydrogen exchange was reported.

2.3 Preparation of Group 5 *ansa*-Metallocene Tetrahydroborate Complexes

2.3.1 Preparation of $[Nb\{(\eta-C_5H_4)C_2Me_4(\eta-C_5H_4)\}Cl_2]$ (1)

A method analogous to that used in the preparation of Group 6 *ansa*-metallocenes was employed to synthesise the dichloride $[Nb\{(\eta-C_5H_4)C_2Me_4(\eta-C_5H_4)\}Cl_2]$ **(1)**.[21-23] The two solids $NbCl_4.2THF$ and $[(MgCl)_2\{(C_5H_4)C_2Me_4(C_5H_4)\}.4THF]$[24] were stirred

together in diethyl ether for 3 days (**Scheme 2.1**). Extraction into dichloromethane followed by washing with pentane yields the compound **1** as a pale brown solid in 70 % yield. This yield compares favourably with that reported for $[Nb\{(\eta-C_5H_4)CMe_2(\eta-C_5H_4)\}Cl_2]$ (55 %). The insoluble material remaining after extraction into dichloromethane is assumed to be oligomeric or polymeric in nature.

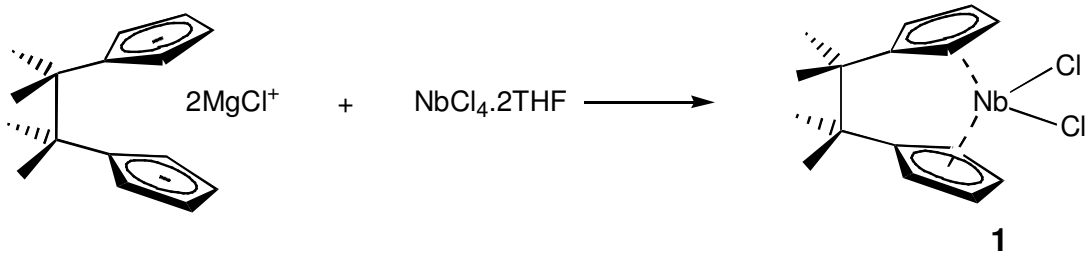

1

Scheme 2.1 Preparation of $[Nb\{(\eta-C_5H_4)C_2Me_4(\eta-C_5H_4)\}Cl_2]$ **(1)**

The compound **1** was characterised by elemental analysis, FAB mass spectrometry and ESR spectroscopy. The FAB mass spectrum shows peaks assigned to the parent ion and the molecular fragment ion resulting from loss of a Cl ligand. The ESR spectrum shows the expected 10 line pattern with g_{iso} = 2.008 and an isotropic coupling constant $|a^{93}Nb|_{iso}$ = 110 G. A similar value for the isotropic coupling constant is reported for the nonbridged species $[Nb(\eta-C_5H_5)_2Cl_2]$ ($|a^{93}Nb|_{iso}$ = 116 G).[25] In contrast, for the single carbon bridged compound $[Nb\{(\eta-C_5H_4)CMe_2(\eta-C_5H_4)\}Cl_2]$ $|a^{93}Nb|_{iso}$ is found to be significantly reduced ($|a^{93}Nb|_{iso}$ = 91 G).[10] The sensitivity of the anisotropic coupling constant to changes in the metallocene geometry is expected in the light of the behaviour of the orbital energies of a metallocene fragment on increased bending of the rings (**Section 1.1.2**).

2.3.2 Preparation of $[Nb\{(\eta-C_5H_4)C_2Me_4(\eta-C_5H_4)\}(\eta^2-BH_4)]$ (2)

Treatment of the compound **1** with excess lithium borohydride in DME at room temperature gives green, air-sensitive crystals of the compound $[Nb\{(\eta-C_5H_4)C_2Me_4(\eta-C_5H_4)\}(\eta^2-BH_4)]$ **(2)** (**Scheme 2.2**). Elemental analyses were fully consistent with the proposed empirical formula.

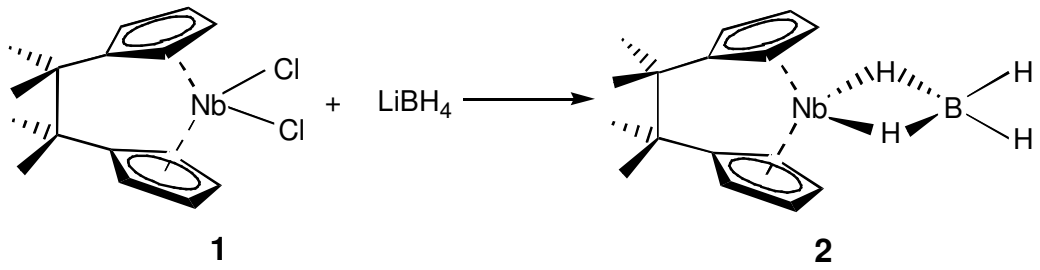

1 **2**

Scheme 2.2 Preparation of [Nb{(η–C_5H_4)C_2Me_4(η–C_5H_4)}(η^2–BH_4)] (**2**)

The IR spectrum of the compound **2** shows two bands in the terminal B-H region at 2465 cm^{-1} and 2427 cm^{-1} and two bands in the bridging M-H-B region at 1712 cm^{-1} and 1661 cm^{-1}. The bands were assigned by analogy to [Nb(η–C_5H_5)$_2$(η^2–BH_4)] and are consistent with a bidentate η^2-BH_4 binding mode.[8] Covalent interaction between the metal and the BH_4 unit is implied by the difference in energy between the B-H_t and B-H_b stretches with the terminal B-H bond stretches being higher energy motions.

The room temperature ^{1}H NMR (C_6D_6) spectrum of the compound **2** shows two partial triplets at δ 5.66 and 5.52 ppm corresponding to the protons of the cyclopentadienyl rings. The protons of the tetramethylethylene bridging unit are assigned to a singlet at δ 0.36 ppm. The protons of the tetrahydroborate ligand were not located in the room temperature spectrum, indicating that the rate of exchange of the bridging and terminal hydrogens lies between the fast and slow exchange limits at this temperature.

The ^{13}C{^{1}H} NMR spectrum of the compound **2** consists of singlets at δ 103.1 and 85.2 ppm assigned to the proton-bearing carbons of the cyclopentadienyl ring, a singlet at δ 43.8 ppm assigned to the quaternary carbon of the bridging C_2Me_4 unit and a further singlet at δ 26.4 ppm corresponding to the methyl carbons of the C_2Me_4 unit. The *ipso*-carbon of the cyclopentadienyl rings was not located. The proton-coupled ^{11}B spectrum of **2** shows a quintet centred at δ 26.9 ppm ($^1J_{BH}$ = 86 Hz).

Partial variable temperature ^{1}H NMR ($C_6D_5CD_3$) spectra between 183 and 363 K for the ethylene-bridged compound **2** are shown in **Figure 2.4**. At high temperature exchange is fast on the NMR time scale and a single broad resonance is observed at δ -5.0 ppm. As temperature is decreased this resonance broadens until coalescence occurs at T_c = 308 ± 3 K. Below the coalescence temperature T_c two singlets are observed at δ 5.3 ppm and -14.9 ppm due to the terminal and bridging hydrogens of the η^2-BH_4 unit

respectively. These two resonances sharpen as the temperature is reduced, although it should be noted that the resonance due to the terminal hydrogens (fwhh = 70 Hz at 198 K) is broader than the high field resonance due to the bridging hydrogens (fwhh = 38 Hz at 198 K).

From the variable temperature ^{1}H NMR study the free energy barrier $\Delta G^{\ddagger}$ to bridge-terminal hydrogen exchange at the coalescence temperature can be calculated according to equation 2.1.

$$\Delta G^{\ddagger} \text{ (kJ mol}^{-1}) = 10^{-3}[RT_c(22.96 + \ln(T_c/\Delta\nu))] \qquad (2.1)$$

For the compound **2** a free energy barrier to exchange of $\Delta G^{\ddagger} = 49.9 \pm 1$ kJ mol^{-1} is determined. $\Delta G^{\ddagger}$ is reduced for the compound **2** compared to that reported for the nonbridged species $[Nb(\eta\text{–}C_5H_5)_2(\eta^2\text{–}BH_4)]$ ($\Delta G^{\ddagger} = 61.1 \pm 1$ kJ mol^{-1}) and $[Nb(\eta\text{–}C_5Me_5)_2(\eta^2\text{-}BH_4)]$ ($\Delta G^{\ddagger} = 68.6 \pm 2$ kJ mol^{-1}).[26]

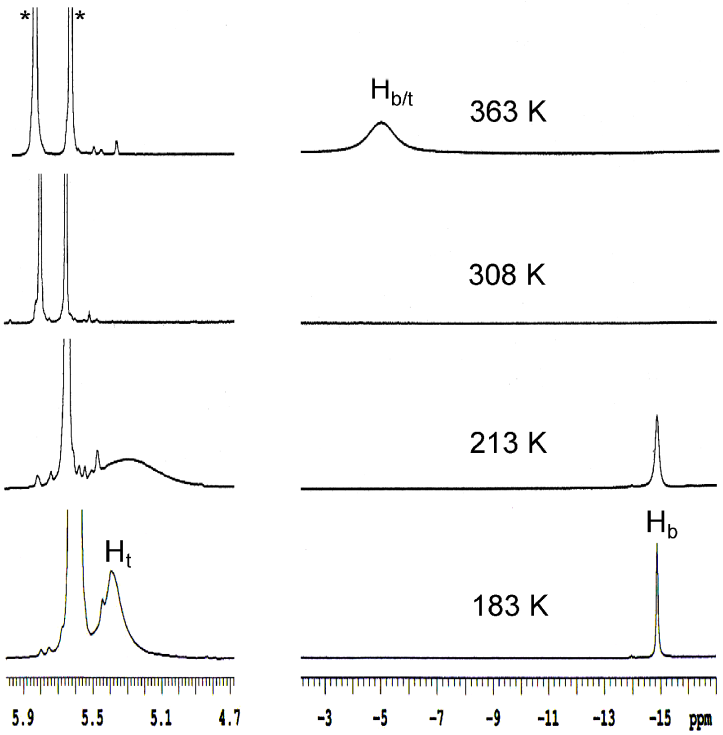

Figure 2.4 Partial variable temperature 500 MHz ^{1}H NMR spectra of $[Nb\{(\eta\text{–}C_5H_4)C_2Me_4(\eta\text{–}C_5H_4)\}(\eta^2\text{–}BH_4)]$ (**2**) in $C_6D_5CD_3$. Peaks due to the protons of the cyclopentadienyl rings are denoted * in the spectrum at 363 K.

Slow cooling of a concentrated solution of the tetrahydroborate complex **2** in petroleum ether (b. p. 100-120 °C) to -80 °C afforded single crystals suitable for X-ray molecular structure determination. The crystal structure was determined and the molecular structure is shown in **Figure 2.5**. Selected interatomic distances and angles and other structural information are presented in **Table 2.1**. Full details of the structure determination are given in **Appendix A**. The compound crystallises in the triclinic space group PI. Hydrogen atoms bound to boron were located in the final difference map and their positions refined.

The bridging B-H_b bonds are longer than the terminal B-H_t bonds confirming the assignment of bidentate ligation of the tetrahydroborate unit and consistent with covalent interaction between the metal and BH_4 ligand. This is also implied by the higher energy B-H_t stretches compared to the B-H_b stretches in the IR spectrum. The bending angle β = 127.1° is similar to that found in the analogous nonbridged compound for $[Nb(\eta\text{–}C_5H_5)_2(\eta^2\text{–}BH_4)]$ (β = 129.8°).[27] This is expected in the light of other structural studies on *ansa*-metallocenes where an ethylene-bridge is found to impose little structural change on the position of the cyclopentadienyl rings relative to the metal, compared to a nonbridged metallocene (**Section 1.3**).[23, 28]

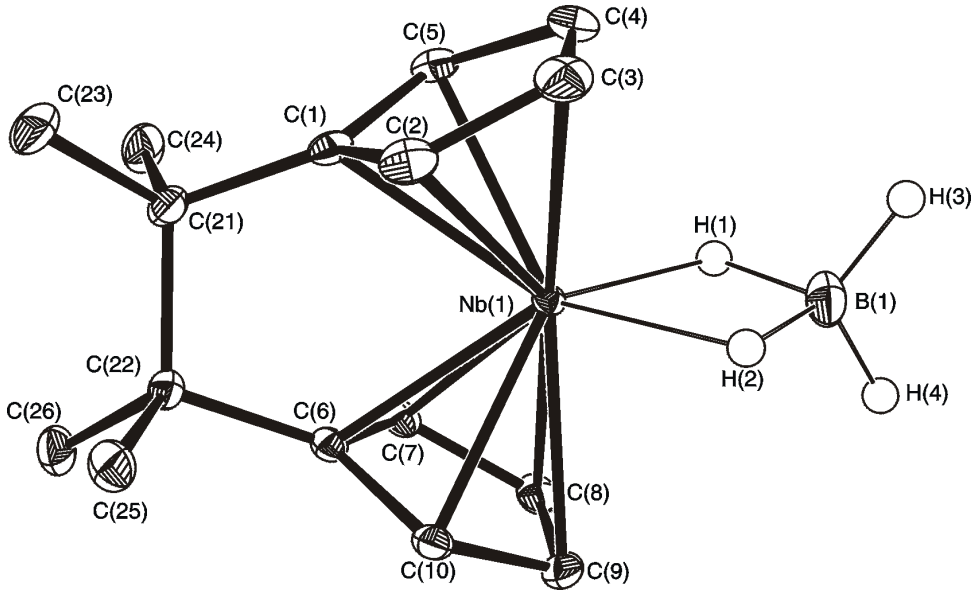

Figure 2.5 Molecular structure of $[Nb\{(\eta-C_5H_4)C_2Me_4(\eta-C_5H_4)\}(\eta^2-BH_4)]$ **(2).** Hydrogen atoms attached to carbon atoms are omitted for clarity.

	Length / Å		Angle / °
Nb-Cp^1_{cent}	2.0240	Between Cp planes, α	52.2
Nb-Cp^1_{ave}	2.3584(14)	Cp^1_{norm}-Nb-Cp^2_{norm}, β	127.8
Nb-Cp^2_{cent}	2.030	Cp^1_{cent}-Nb-Cp^2_{cent}, χ	134.38
Nb-Cp^2_{ave}	2.3644(14)	C_{ipso}-Cp plane, ϕ	-2.4, -2.6
Nb-C(1)	2.3041(13)		
Nb-C(3)	2.4274(15)		
C_{ipso}-C_{ipso}	2.6835		
Nb-H(1)	1.81(2)		
B-H(1)	1.28(2)		
B-H(3)	1.12(3)		

Cp^1 = Ring C(1)-C(5), Cp^2 = Ring C(6)-C(10)

Table 2.1 Selected interatomic distances and angles and other structural information for $[Nb\{(\eta-C_5H_4)C_2Me_4(\eta-C_5H_4)\}(\eta^2-BH_4)]$ **(2)**

There is a small departure in planarity at the *ipso*-carbons in the compound **2** (ϕ *ca* -2.5°). In contrast to the single atom-bridged compound [Nb{(η–C_5H_4)CMe_2(η–C_5H_4)}(η^2–BH_4)] the *ipso*-carbon vector lies above the plane of the cyclopentadienyl rings reflecting the steric demand of a two-carbon bridge.[10] In the compound **2** the *ipso*-carbons and the carbons of the bridge are not coplanar, corresponding to a twisting of the bridging unit (**Figure 2.6**).

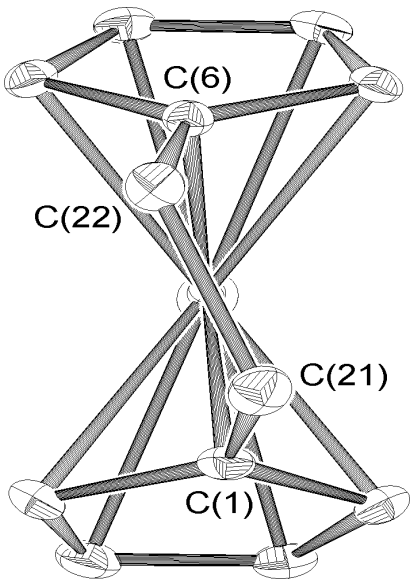

Figure 2.6 Alternative view of the molecular structure of [Nb{(η–C_5H_4)C_2Me_4(η–C_5H_4)}(η^2–BH_4)] **(2).** Methyl groups on the bridging unit and hydrogen atoms are omitted for clarity.

2.3.3 Preparation of [Nb{(η–C_5H_4)C_2Me_4(η–C_5H_4)}(η^2–BD_4)] (3)

In an attempt to further investigate the mechanism of bridge-terminal hydrogen exchange in tetrahydroborate derivatives, the tetradeuteroborate analogue of the compound **2**, [Nb{(η–C_5H_4)C_2Me_4(η–C_5H_4)}(η^2–BD_4)] **(3)** was prepared by the action of sodium borodeuteride on the compound **1** (**Scheme 2.3**). The effect of isotopic substitution on the free energy barrier to exchange in tetrahydroborate derivatives has not been previously reported.

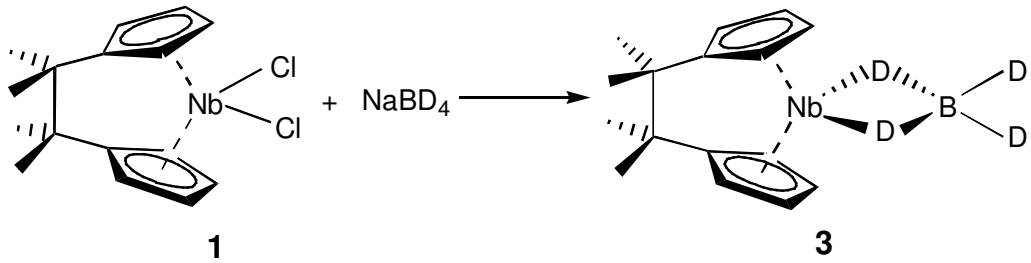

1 **3**

Scheme 2.3 Preparation of $[Nb\{(\eta-C_5H_4)C_2Me_4(\eta-C_5H_4)\}(\eta^2-BD_4)]$ **(3)**

The compound **3** was characterised by IR spectroscopy, ^1H, ^2H, $^{13}C\{^1H\}$ and ^{11}B NMR spectroscopy and elemental analysis. As expected the B-D stretching frequencies are found at lower energy than the corresponding B-H stretches in the compound **2** and are assigned by analogy to $[V(\eta-C_5H_5)_2(\eta^2-BD_4)]$.[8] The symmetric and asymmetric B-D_t stretching frequencies occur at 1880 and 1769 cm^{-1}. Only one of the B-D_b stretches could be located at 1261 cm^{-1}.

The room temperature NMR spectra of the compound **3** are essentially the same as for the compound **2**. However the ^{11}B NMR spectrum consists of a broad singlet at δ 25.5 ppm. The dynamic processes in the tetradeuteroborate unit were investigated by variable temperature ^2H NMR ($C_6H_5CH_3$) spectroscopy. At 373 K a single resonance is observed at δ -4.9 ppm consistent with bridge-terminal deuterium exchange being fast on the NMR time scale. As temperature is lowered this resonance broadens until coalescence occurs at $T_c = 278 \pm 5$ K, corresponding to a free energy barrier at the coalescence temperature of $\Delta G^{\ddagger} = 49.1 \pm 2$ kJ mol^{-1}. Within experimental error this is essentially the same as for that observed for the compound **2** ($\Delta G^{\ddagger} = 49.9 \pm 1$ kJ mol^{-1}). In the slow exchange limit two singlets are observed at δ 4.9 and -15.3 ppm assigned to the terminal and bridging deuteriums respectively.

2.3.4 Preparation of $[Nb\{(\eta-C_5H_3\text{-}^tBu)C_2Me_4(\eta-C_5H_3\text{-}^tBu)\}Cl_2]$ (4)

It was decided to investigate the possibility of inductive electronic effects influencing the dynamic properties of *ansa*-metallocene tetrahydroborate complexes. To this end the ^{t}Bu substituted precursor $[Nb\{(\eta-C_5H_3\text{-}^tBu)C_2Me_4(\eta-C_5H_3\text{-}^tBu)\}Cl_2]$ **(4)** was prepared by the reaction between $NbCl_4.2THF$ and $[(MgCl)_2\{(C_5H_3\text{-}^tBu)C_2Me_4(C_5H_3\text{-}^tBu)\}.4THF]$[29] in an analogous procedure to that used to prepare the compound **1**

(**Scheme 2.4**). The presence of the ^{t}Bu groups on the cyclopentadienyl rings might be expected to increase the electron density at the metal centre and thus have some effect on the free energy barrier to bridge-terminal hydrogen exchange in the tetrahydroborate derivative.

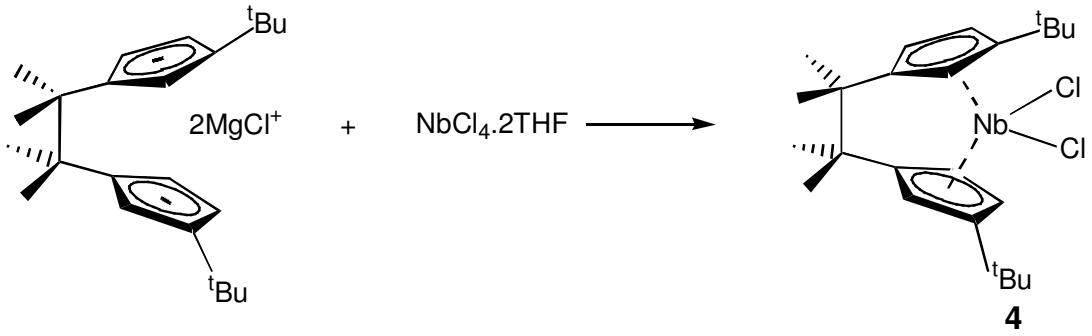

4

Scheme 2.4 Preparation of [Nb{(η–C_5H_3-^{t}Bu)C_2Me_4(η–C_5H_3-^{t}Bu)}Cl_2] **(4)**

The crude product **4** was obtained as a brown powder in 74 % yield and was used in subsequent reactions. An analytically pure sample of the compound **4** was obtained by sublimation at 160 °C (10^{-1} mm Hg). The compound **4** was further characterised by ESR spectroscopy and FAB mass spectrometry. The ESR spectrum of the compound **4** is analogous to that for the compound **1** with g_{iso} = 1.987 and $|a^{93}Nb|_{iso}$ = 112 G. The FAB mass spectrum of the compound **4** shows a peak due to the parent ion and peaks corresponding to the consecutive loss of one and two Cl ligands. The compound **4** is expected to consist of a mixture of *rac*- and *meso*-isomers, although no information regarding the relative proportions of each was obtained.

2.3.5 Preparation of [Nb{(η–C_5H_3-^{t}Bu)C_2Me_4(η–C_5H_3-^{t}Bu)}(η^2–BH_4)] (5)

The substituted *ansa*-metallocene tetrahydroborate compound [Nb{(η–C_5H_3-^{t}Bu)C_2Me_4(η–C_5H_3-^{t}Bu)}(η^2–BH_4)] **(5)** was prepared by the reaction between the compound **4** and lithium borohydride (**Scheme 2.5**). The compound **5** is obtained as dark green crystals after recrystallisation from petroleum ether (b. p. 100 – 120 ºC) with a *rac:meso* ratio of 3:2. The *rac*-isomer is expected to predominate on steric grounds. Indeed in the case of the first-row *ansa*-metallocenes

[M{(η–C_5H_3-^{t}Bu)C_2Me_4(η–C_5H_3-^{t}Bu)}] (M = Fe, Co) only the *rac*-isomer is isolated.[29] Repeated recrystallisation of the compound **5** allows the *rac*-isomer to be isolated.

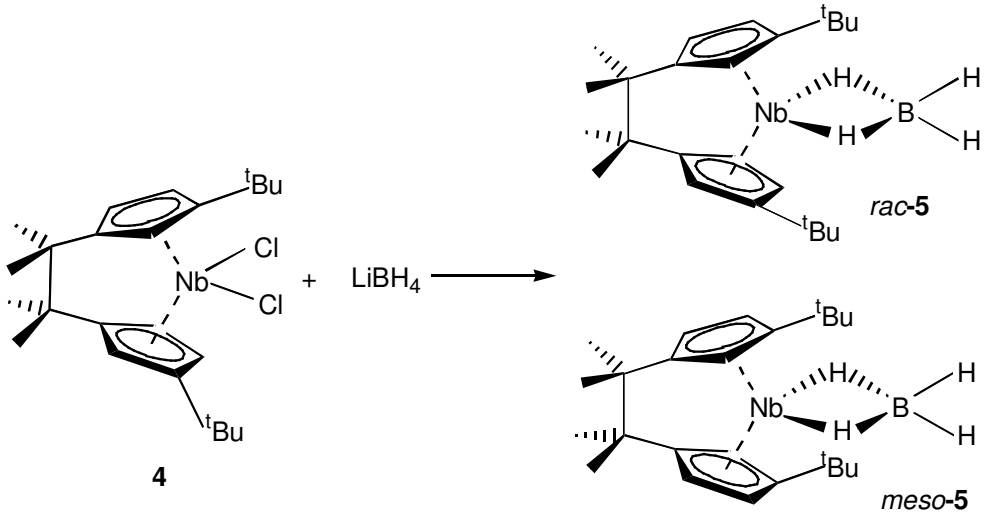

Scheme 2.5 Preparation of [Nb{(η–C_5H_3-^{t}Bu)C_2Me_4(η–C_5H_3-^{t}Bu)}(η^2–BH_4)] **(5)**

The *rac*-isomer of the compound **5** was characterised by IR spectroscopy, ^{1}H, ^{13}C{^{1}H} and ^{11}B NMR spectroscopy and elemental analysis. The IR spectrum of *rac*-**5**, recorded as a Nujol mull, shows two bands in the terminal B-H region at 2467 cm^{-1} and 2430 cm^{-1} and two bands in the bridging B-H region at 1690 cm^{-1} and 1666 cm^{-1}. These are in close agreement to those found for the compound **2**.

The ^{1}H NMR spectrum of *rac*-**5** consists of three singlets at δ 6.22, 5.37 and 5.26 ppm corresponding to the three protons of the cyclopentadienyl rings. The protons of the ^{t}Bu groups occur as a singlet at δ 1.40 ppm and the protons of the tetramethylethylene bridge occur as a pair of singlets at δ 0.53 and 0.49 ppm. The ^{13}C{^{1}H} and ^{11}B NMR spectra are straightforward and not discussed here. The *meso*-isomer of the compound **5** was characterised by ^{1}H, ^{13}C{^{1}H} and ^{11}B NMR spectrsoscopy only. The assignment of peaks in the ^{13}C{^{1}H} NMR spectra of *rac*- and *meso*-**5** were confirmed by a ^{1}H-^{13}C NMR shift correlation experiment.

Bridge-terminal hydrogen exchange in *rac*-**5** was investigated by variable temperature ^{1}H NMR spectroscopy. At 363 K the exchange is fast on the NMR time scale and a single broad resonance is observed at δ -4.5 ppm. As temperature is decreased this resonance broadens until coalescence occurs at T_c = 303 ± 3 K, corresponding to a free energy barrier to exchange of $\Delta G^{\ddagger}$ = 49.1 ± 1 kJ mol^{-1}. The value of $\Delta G^{\ddagger}$ at T_c for the

compound **2** is 49.9 ± 1 kJ mol^{-1}. Below the coalescence temperature T_c two singlets are observed at δ 5.2 ppm and -13.9 ppm due to the terminal and bridging hydrogens of the η^2-BH_4 unit respectively.

Slow cooling of a concentrated solution of *rac*-**5** in petroleum ether (b. p. 100 – 120 °C) afforded single crystals suitable for X-ray structural analysis. The crystal structure was determined and the molecular structure is shown in **Figure 2.7**. Selected interatomic distances and angles and other structural information are presented in **Table 2.2**. Full details of the structure determination are given in **Appendix B**. The compound crystallises in the triclinic space group PI. Hydrogen atoms bound to boron were located in the final difference map and their positions were refined.

The molecular structure of *rac*-**5** shows the *exo*-configuration of the ^{t}Bu groups. As expected the structural features of the metallocene fragment are closely similar to those seen in the nonsubstituted analogue **2**, although the bending angles α and β differ from those in the compound **2** by 3.1°. As for the compound **2**, the nonplanarity of the atoms C(1), C(6), C(21) and C(22) corresponds to a twisting of the bridging tetramethyethylene unit.

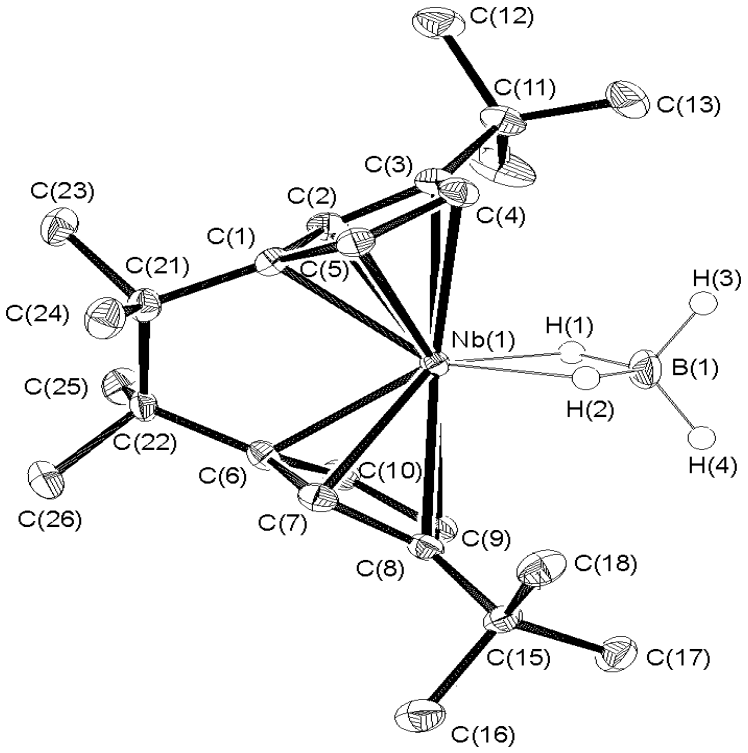

Figure 2.7 Molecular structure of *rac*-[Nb{(η–C_5H_3-^{t}Bu)C_2Me_4(η–C_5H_3-^{t}Bu)}(η^2–BH_4)] **(5).** Hydrogen atoms attached to carbon atoms are omitted for clarity.

	Length / Å		Angle / °
Nb-Cp^1_{cent}	2.0493	Between Cp planes, α	55.3
Nb-Cp^1_{ave}	2.3800(18)	Cp^1_{norm}-Nb-Cp^2_{norm}, β	124.7
Nb-Cp^2_{cent}	2.0478	Cp^1_{cent}-Nb-Cp^2_{cent}, χ	133.6
Nb-Cp^2_{ave}	2.3796(18)	C_{ipso}-Cp plane, ϕ	-4.8, -3.4
Nb-C(1)	2.299(3)		
Nb-C(3)	2.497(3)		
C_{ipso}-C_{ipso}	2.6649		
Nb-H(1)	1.89(5)		
B-H(1)	1.17(5)		
B-H(3)	1.10(5)		

Cp^1 = Ring C(1)-C(5), Cp^2 = Ring C(6)-C(10)

Table 2.2 Selected interatomic distances and angles and other structural information for [Nb{(η–C_5H_3-^{t}Bu)C_2Me_4(η–C_5H_3-^{t}Bu)}(η^2–BH_4)] **(5)**

2.3.6 Preparation of [Nb{(η–C_5H_4)$SiMe_2$(η–C_5H_4)}Cl_2]

Otero *et al.* have described the synthesis of [Nb{(η–C_5H_4)$SiMe_2$(η–C_5H_4)}Cl_2] by the reaction between $NbCl_4$.2THF and [Tl_2{(C_5H_4)$SiMe_2$(C_5H_4)}] in THF.[20] The thallium reagent rather than the lithium reagent was employed because the reaction between $NbCl_4$.2THF and [Li_2{(C_5H_4)$SiMe_2$(C_5H_4)}] in THF gave diminished yields, which was attributed to reduction processes. Using the reagent [Li_2{(C_5H_4)$SiMe_2$(C_5H_4)}][30] in a reaction analogous to that used to prepare the compounds **1** and **4** gives [Nb{(η–C_5H_4)$SiMe_2$(η–C_5H_4)}Cl_2] in 36% yield (**Scheme 2.6**).

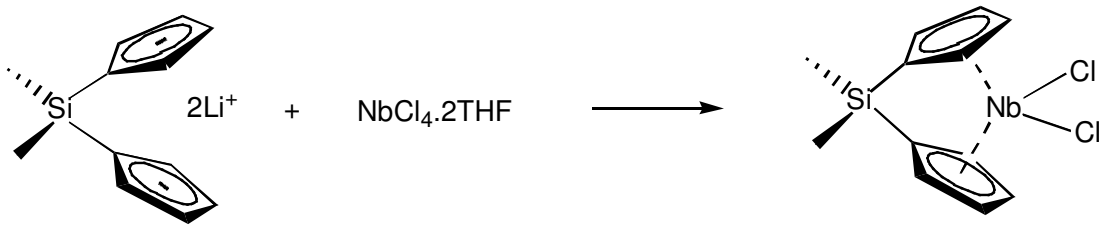

Scheme 2.6 Preparation of [Nb{(η–C_5H_4)$SiMe_2$(η–C_5H_4)}Cl_2]

2.3.7 Preparation of [Nb{(η–C_5H_4)$SiMe_2$(η–C_5H_4)}(η^2–BH_4)] (6)

The silicon-bridged tetrahydroborate derivative [Nb{(η–C_5H_4)$SiMe_2$(η–C_5H_4)}(η^2–BH_4)] **(6)** was prepared by the action of lithium borohydride on a suspension of the compound [Nb{(η–C_5H_4)$SiMe_2$(η–C_5H_4)}Cl_2] in DME (**Scheme 2.7**). As for the compounds **2** and **4**, the compound **6** was extracted from the reaction mixture into petroleum ether (b. p. 100 - 120 °C) and isolated as a dark green crystalline solid.

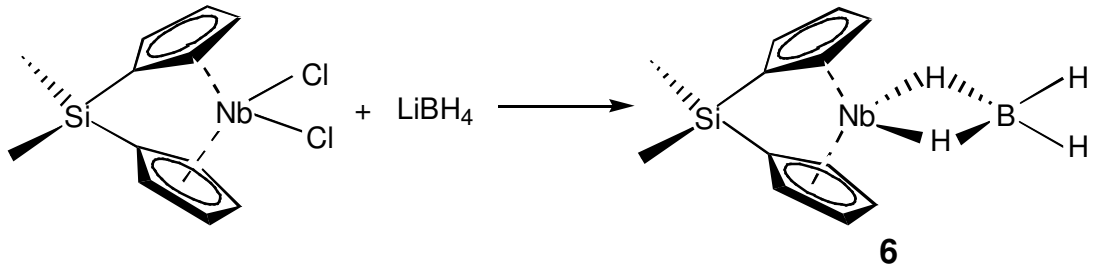

Scheme 2.7 Preparation of [Nb{(η–C_5H_4)$SiMe_2$(η–C_5H_4)}(η^2–BH_4)] **(6)**

The tetrahydroborate compound **6** was fully characterised by elemental analysis, IR spectroscopy, ^{1}H, $^{13}C\{^{1}H\}$ and ^{11}B NMR spectroscopy and FAB mass spectrometry. The IR spectrum shows the expected pair of B-H_t stretches at 2460 and 2410 cm^{-1} and pair of B-H_b stretches at 1703 and 1652 cm^{-1}. The ^{1}H NMR spectrum shows, in addition to partial triplets at δ 6.03 and 5.16 ppm corresponding to the cyclopentadienyl protons, a peak at δ -0.62 ppm due to the methyl protons of the $SiMe_2$ bridge. Again peaks due to the protons of the tetrahydroborate ligand cannot be readily located in the room temperature spectrum, suggesting that at this temperature bridge-terminal hydrogen exchange is intermediate between the fast and slow exchange limits on the NMR time scale.

A variable temperature ^{1}H NMR study allowed elucidation of the free energy barrier to exchange $\Delta G^{\ddagger}$ at the coalescence temperature. At high temperature (*ca*. 363 K) exchange is fast on the NMR time scale and a single broad resonance is observed at δ -5.0 ppm. As temperature is decreased this resonance broadens until coalescence occurs at T_c = 305 ± 3 K, corresponding to $\Delta G^{\ddagger}$ = 49.3 ± 1 kJ mol^{-1}. Thus the influence of a silicon- and ethylene-bridge on the exchange process appears to be very similar ($\Delta G^{\ddagger}$ = 49.3 ± 1 kJ mol^{-1} for the compound **2**). Below the coalescence temperature T_c two singlets are observed at δ 5.5 ppm and -14.9 ppm due to the terminal and bridging hydrogens of the BH_4 unit respectively. These resonances sharpen considerably as temperature is reduced, although the peak due to the bridging hydrogens (fwhh = 69 Hz at 198 K) is broader than that due to the terminal hydrogens (fwhh = 36 Hz at 198 K).

Attempts to characterise the tetrahydroborate derivatives prepared in this work by FAB mass spectrometry were generally unsuccessful. This is most likely to be a result of the extremely air-sensitive nature of the compounds and the method of material manipulation employed in the FAB mass spectrometry technique. The compound **6** was however successfully characterised by FAB mass spectrometry. Peaks due to the parent ion and the fragment ion resulting from loss of the BH_4 ligand are observed.

Slow cooling of a concentrated solution of the tetrahydroborate complex **6** in petroleum ether (b. p. 100-120 °C) to -80 °C afforded single crystals suitable for X-ray molecular structure determination. The crystal structure was determined and the molecular structure is shown in **Figure 2.8**. Selected interatomic distances and angles and other structural information are presented in **Table 2.3**. Full details of the structure determination are given in **Appendix C**. The compound crystallises in the monoclinic

space group $P2_1/n$. Hydrogen atoms bound to boron were located in the final difference map and their positions refined.

The molecular structure of the compound **6** shows similar structural features to the ethlylene-bridged compounds **2** and *rac*-**5**. In particular the bending angle β is 127.2°, compared to 127.8° and 124.7° for the ethylene-bridged compounds **2** and *rac*-**5** respectively and 129.8° for the nonbridged compound $[Nb(\eta-C_5H_5)_2(\eta^2-BH_4)]$. Thus as observed in other series of *ansa*-metallocenes a silicon- and ethylene-bridge has little influence on the position of the cyclopentadienyl rings relative to the metal.[23, 28] As expected the bridging B-H_b bond B-H(1) is longer than the terminal B-H_t bond B-H(3). There is significant deviation from planarity at the *ipso*-carbon in the compound **6** (ϕ *ca.* 20.6°). This deviation is much greater than seen in the compounds **2** and *rac*-**5** and can be attributed to the fact that the bridging unit is a single atom. Furthermore, whereas the ethylene-bridge forces a deviation of the C_{ipso} vector above the plane of the cyclopentadienyl ring, in the case of the compound **6** the C_{ipso} vector lies below the ring plane.

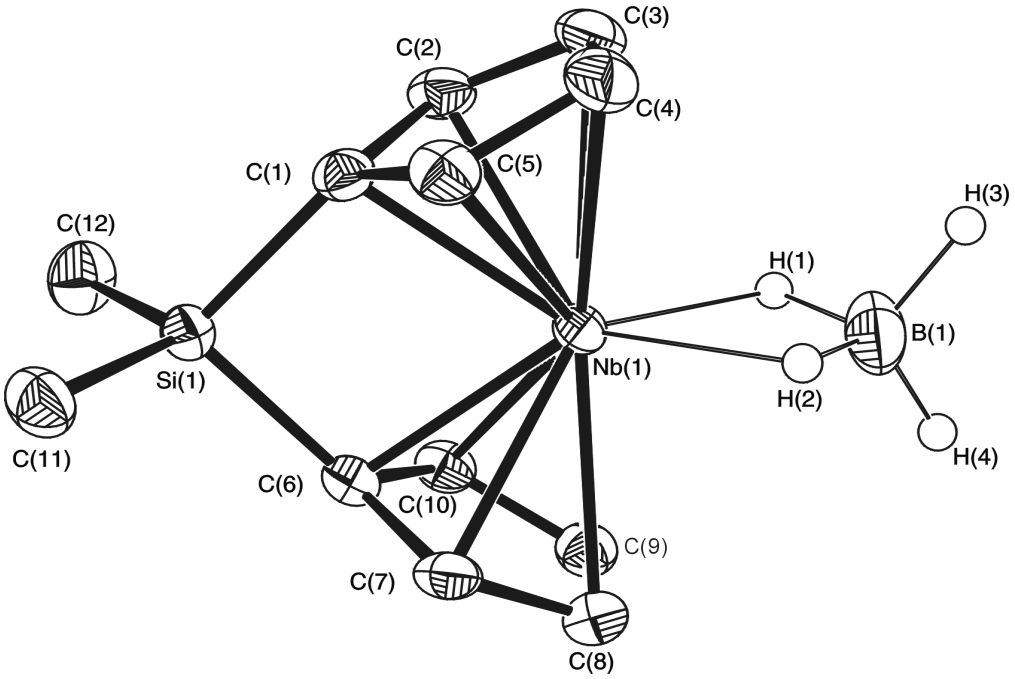

Figure 2.8 Molecular structure of $[Nb\{(\eta-C_5H_4)SiMe_2(\eta-C_5H_4)\}(\eta^2-BH_4)]$ **(6).** Hydrogen atoms attached to carbon atoms are omitted for clarity.

	Length / Å		Angle / °
Nb-Cp^1_{cent}	2.0350	Between Cp planes, α	52.8
Nb-Cp^1_{ave}	2.365(4)	Cp^1_{norm}-Nb-Cp^2_{norm}, β	127.2
Nb-Cp^2_{cent}	2.0329	Cp^1_{cent}-Nb-Cp^2_{cent}, χ	135.7
Nb-Cp^2_{ave}	2.367(3)	C_{ipso}-Cp plane, ϕ	20.8, 20.4
Nb-C(1)	2.307(3)	C_{ipso}-Si-C_{ipso}, ε	92.8
Nb-C(3)	2.429(4)		
C_{ipso}-C_{ipso}	2.6991		
Nb-H(1)	1.92(5)		
B-H(1)	1.24(5)		
B-H(3)	1.11(3)		

Cp^1 = Ring C(1)-C(5), Cp^2 = Ring C(6)-C(10)

Table 2.3 Selected interatomic distances and angles and other structural information for $[Nb\{(\eta-C_5H_4)SiMe_2(\eta-C_5H_4)\}(\eta^2-BH_4)]$ **(6)**

2.3.8 Preparation of [Nb{(η–C_5H_4)CEt_2(η–C_5H_4)}Cl_2] (7)

In order to study the effect of a single carbon atom bridge on the bridge-terminal hydrogen exchange process in niobocene tetrahydroborate derivatives, the dichloride precursor [Nb{(η–C_5H_4)CEt_2(η–C_5H_4)}Cl_2] **(7)** was prepared. The compound [Nb{(η–C_5H_4)CMe_2(η–C_5H_4)}Cl_2] was previously prepared in this laboratory *via* the addition of a suspension of [K_2{(C_5H_4)CMe_2(C_5H_4)}] in THF to a suspension of $NbCl_4$.2THF in THF.[10] In an analogous procedure the compound **7** was prepared by the reaction between $NbCl_4$.2THF and [Li_2{(C_5H_4)CEt_2(ηC$_5H_4$)}] (**Scheme 2.8).** The compound **7** was isolated by extraction into toluene as a dark brown solid in 37 % yield. An analytically pure sample of the compound **7** was obtained by sublimation at 165 °C (10^{-1}mmHg).

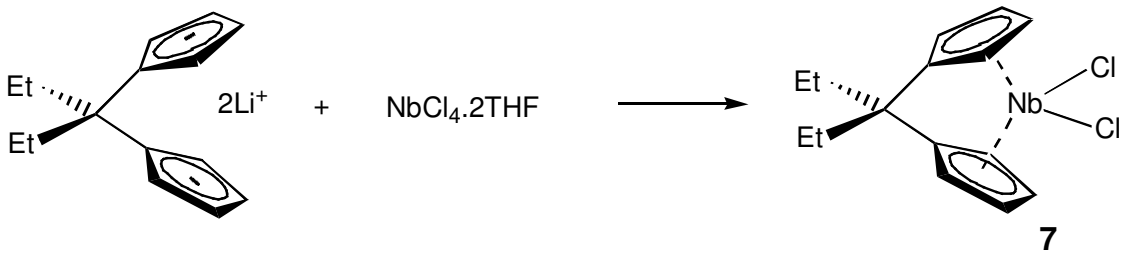

Scheme 2.8 Preparation of [Nb{(η–C_5H_4)CEt_2(η–C_5H_4)}Cl_2] **(7)**

The compound **7** was also characterised by FAB mass spectrometry and ESR spectroscopy. The FAB mass spectrum of the compound **7** shows a peak corresponding to the molecular ion and a fragment peak due to loss of a Cl ligand from the molecular ion. The ESR spectrum shows the familiar 10 line pattern for an unpaired electron mainly located at the ^{93}Nb (I = $^9/_2$) nucleus, with a value of g_{iso} = 1.998 and a hyperfine splitting $|a^{93}Nb|_{iso}$ = 94 G. As discussed in **Section 2.3.1**, there is significant reduction in the isotropic coupling constant $|a^{93}Nb|_{iso}$ for single carbon atom bridged niobocene dichlorides compared to the analogous ethylene-bridged (**1** and **4**) and nonbridged species.

2.3.9 Preparation of [Nb{(η–C_5H_4)CEt_2(η–C_5H_4)}(η^2–BH_4)] (8)

The tetrahydroboroate complex [Nb{(η–C_5H_4)CEt_2(η–C_5H_4)}(η^2–BH_4)] **(8)** was prepared by the reaction between the crude product **7** and lithium borohydride in a procedure analogous to that used to prepare the tetrahydroborate compounds **2, 5** and **6**

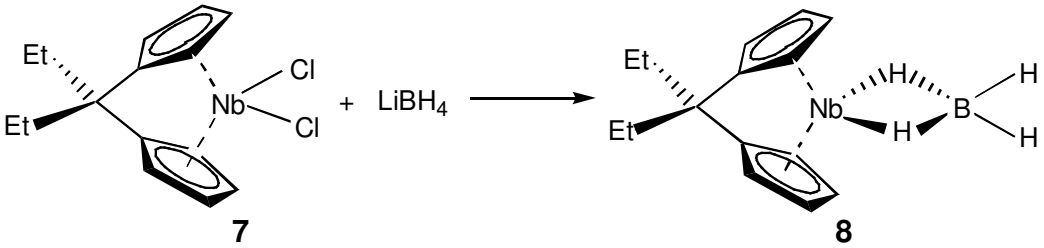

7 **8**

(**Scheme 2.9**).

Scheme 2.9 Preparation of [Nb{(η–C_5H_4)CEt_2(η–C_5H_4)}(η^2–BH_4)] **(8)**

The compound **8** was fully characterised by the methods described in the preceeding sections. Of particular note is the room temperature ^{1}H NMR spectrum of the compound **8**. In this case a broad resonace is observed at δ -3.5 ppm corresponding to the protons of the BH_4 unit, implying that exchange is fast at room temperature on the NMR time scale. It can be concluded that the free energy barrier to bridge-terminal hydrogen exchange $\Delta G^{\ddagger}$ is considerably smaller than for the ethylene- and silicon-bridged compounds **2, 4** and **6** and the analogous nonbridged compound [Nb(η–C_5H_5)$_2$(η^2–BH_4)].

This assumption is verified by a variable temperature ^{1}H NMR study of the compound **8**. Coalescence is not observed until the temperature is lowered to 223 ± 3 K corresponding to a free energy barrier at the coalescence temperature of $\Delta G^{\ddagger}$ = 35.8 ± 1 kJ mol^{-1}. On further cooling to 183 K two broad resonances appear at δ 5.3 and -11.6 ppm corresponding to the terminal and bridging protons respectively.

Single crystals suitable for X-ray molecular structure determination were obtained by the slow cooling of a concentrated petroleum ether (b. p. 100-120°) solution to -80 °C. The crystal structure was determined and the molecular structure is shown in **Figure 2.9**. Selected interatomic distances and angles and other structural information are presented in **Table 2.4**. Full details of the structure determination are given in **Appendix D**. The compound crystallises in the monoclinic space group $P2_1/n$. Hydrogen atoms bound to boron were located in the final difference map and their positions refined.

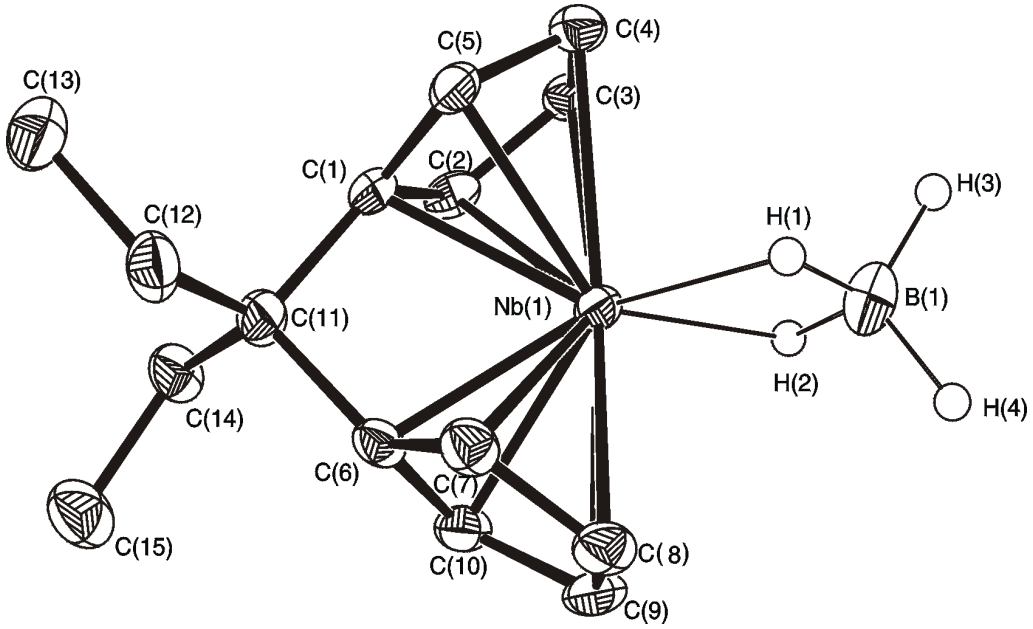

Figure 2.9 Molecular structure of $[Nb\{(\eta-C_5H_4)CEt_2(\eta-C_5H_4)\}(\eta^2-BH_4)]$ **(8).** Hydrogen atoms attached to carbon atoms are omitted for clarity.

	Length / Å		Angle / °
$Nb\text{-}Cp^1_{cent}$	2.0076	Between Cp planes, α	64.4
$Nb\text{-}Cp^1_{ave}$	2.344(4)	$Cp^1_{norm}\text{-}Nb\text{-}Cp^2_{norm}$, β	115.6
$Nb\text{-}Cp^2_{cent}$	2.0104	$Cp^1_{cent}\text{-}Nb\text{-}Cp^2_{cent}$, χ	124.98
$Nb\text{-}Cp^2_{ave}$	2.347(4)	C_{ipso}-Cp plane, ϕ	17.2, 17.3
Nb-C(1)	2.280(4)	$C_{ipso}\text{-}C(11)\text{-}C_{ipso}$, ε	97.2(3)
Nb-C(3)	2.423(3)		
$C_{ipso}\text{-}C_{ipso}$	2.22934		
Nb-H(1)	2.04(6)		
B-H(1)	1.25(6)		
B-H(3)	1.16(7)		

Cp^1 = Ring C(1)-C(5), Cp^2 = Ring C(6)-C(10)

Table 2.4 Selected interatomic distances and angles and other structural information for $[Nb\{(\eta-C_5H_4)CEt_2(\eta-C_5H_4)\}(\eta^2-BH_4)]$ **(8).**

As is immediately evident from inspection of the molecular structure of the compound **8**, the presence of a single carbon bridge has a significant influence on the geometry of the metallocene unit. In particular the angle between the Cp rings, α, is increased by *ca* 12° relative to the compounds **2**, *rac*-**5** and **6** and by *ca* 14° compared to the analogous nonbridged compound [Nb(η–C_5H_5)$_2$(η^2–BH_4)]. Consequently the bending angle β is reduced and can be interpreted as the *ansa*-bridge 'bending back' the cyclopentadienyl rings from the metal centre.

Recent density functional studies have shown that as the angle between the rings, α, is increased two of the metal d-orbitals become more involved in metal-ring bonding, primarily at the *ipso*-carbon (**Section 4.2.7**).[31] **Figure 2.10** shows that the Nb-C_{ipso} distance is shorter than the other Nb-C distances. Furthermore the C-C bond opposite the *ipso*-carbon is the shortest of the inter ring C-C distances. Equality of C-C bond lengths around the cyclopentadienyl ring is indicative of an η^5-mode of coordination. Thus it can be concluded that the presence of a single-carbon bridge causes the metal to lie closer to the *ipso*-carbons and that there is a significant contribution to π bonding in the cyclopentadienyl rings from an η^3-allyl resonance structure.

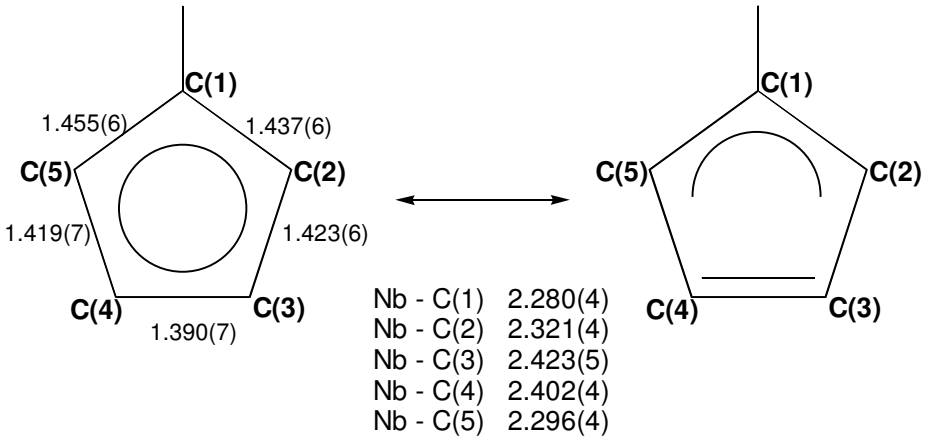

Figure 2.10 Structural parameters associated with the bonding of the cyclopentadienyl rings in [Nb{(η–C_5H_4)CEt_2(η–C_5H_4)}(η^2–BH_4)] **(8)**

2.3.10 Reinvestigation of the Dynamic Properties of [Nb{(η–C_5H_4)CMe_2(η–C_5H_4)}(η^2–BH_4)]

An earlier study of the dynamic properties of the compound [Nb{(η–C_5H_4)CMe_2(η–C_5H_4)}(η^2–BH_4)] *via* variable temperature ^{1}H NMR spectroscopy reported that the exchange of bridging and terminal hydrogens was fast even at 183 K.[10] Since the current dynamic studies and those reported for [Nb{(η–C_5H_4)CMe_2(η–C_5H_4)}(η^2–BH_4)] were carried out on a 500 MHz spectrometer and in the same solvent ($C_6D_5CD_3$), and particularly in the light of the results of the study of the compound **8**, the dynamic properties described for [Nb{(η–C_5H_4)CMe_2(η–C_5H_4)}(η^2–BH_4)] could not be readily explained.

Thus the compound [Nb{(η–C_5H_4)CMe_2(η–C_5H_4)}(η^2–BH_4)] was prepared and bridge-terminal hydrogen exchange reinvestigated by variable temperature ^{1}H NMR spectroscopy. As expected the dynamic properties are found to be essentially the same as for the compound **8**. At room temperature the exchange is, as previously reported, fast on the NMR time scale with a peak at δ -3.4 ppm. However, on cooling this peak broadens until decoalescence is reached at T_c = 228 ± 3 K. Broad peaks at δ 5.2 and -11.6 ppm corresponding to terminal and bridging hydrogens can be located at 183 K and a free energy barrier of $\Delta G^{\ddagger}$ = 35.0 ± 1 kJ mol^{-1} is calculated. For the analogous compound **8** $\Delta G^{\ddagger}$ = 35.8 ± 1 kJ mol^{-1}.

2.3.11 Preparation of [Nb{(η–C_5H_4)CMe_2(η–C_5H_4)}(η^2–BD_4)] (9)

The study of the dynamic properties of the compounds **2** and **3** shows that there is no observable kinetic isotope effect in the exchange process for ethylene-bridged *ansa*-metallocene tetrahydroborate complexes. Since the reduction in $\Delta G^{\ddagger}$ compared to the nonbridged compound is more marked for the methylene bridged compounds, **8** and [Nb{(η–C_5H_4)CMe_2(η–C_5H_4)}(η^2–BH_4)], than the ethylene-bridged compound **2** it was decided to prepare the isotopically substituted compound [Nb{(η–C_5H_4)CMe_2(η–C_5H_4)}(η^2–BD_4)] **(9)** to investigate whether the barrier to exchange is sensitive to isotopic substitution in this case.

The compound **9** was prepared by the reaction between [Nb{(η–C_5H_4)CMe_2(η–C_5H_4)}Cl_2] and sodium borodeuteride (**Scheme 2.10**).

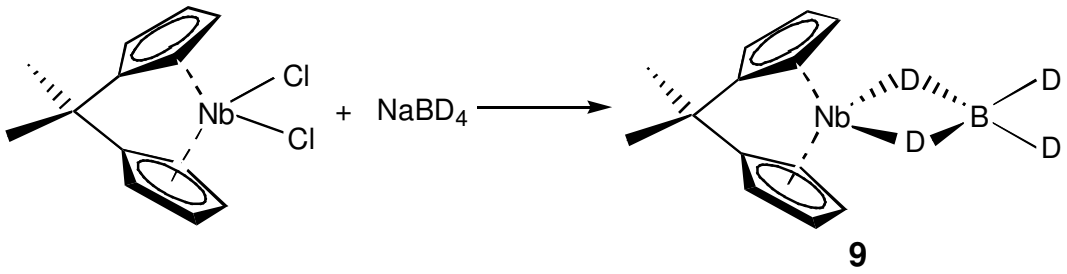

9

Scheme 2.10 Preparation of $[Nb\{(\eta\text{–}C_5H_4)CMe_2(\eta\text{–}C_5H_4)\}(\eta^2\text{–}BD_4)]$ **(9)**

The compound **9** was characterised by elemental analysis, IR spectroscopy and ^1H, ^2H, $^{13}C\{^1H\}$ and ^{11}B NMR spectroscopy. As expected the B-D stretching frequencies are found at lower energy than the corresponding B-H stretches in the compound $[Nb\{(\eta\text{–}C_5H_4)CMe_2(\eta\text{–}C_5H_4)\}(\eta^2\text{–}BH_4)]$. The symmetric and asymmetric $B\text{-}D_t$ stretching frequencies occur at 1860 and 1790 cm^{-1}. Only one of the $B\text{-}D_b$ stretches was located at 1270 cm^{-1}.

The ^{11}B NMR spectrum shows a broad peak at δ -3.0 ppm. The dynamic properties of the BD_4 unit were investigated by variable temperature ^2H NMR (76.75 MHz, $C_6D_5CD_3$) spectroscopy. Coalescence occurs at $T_c = 198 \pm 5$ K, with peaks at δ 4.2 and -12.3 ppm corresponding to the terminal and bridging deuterium appearing in the spectra as the temperature is reduced below T_c. A value of $\Delta G^{\ddagger} = 34.8 \pm 2$ kJ mol^{-1} is deduced. Thus within experimental error there is no observable kinetic isotope effect for the exchange process, as was found for the ethylene-bridged compounds **2** and **3.**

2.3.12 Preparation of $[Nb\{(\eta\text{–}C_5H_4)C(C_5H_{10})(\eta\text{–}C_5H_4)\}Cl_2]$ (10)

A further example of a single carbon-bridged Group 5 *ansa*-metallocene, the compound $[Nb\{(\eta\text{–}C_5H_4)C(C_5H_{10})(\eta\text{–}C_5H_4)\}Cl_2]$ **(10),** was prepared by the reaction between $NbCl_4.2THF$ and $[Li_2\{(C_5H_4)C(C_5H_{10})(\eta C_5H_4)\}]$[22] (**Scheme 2.11).**

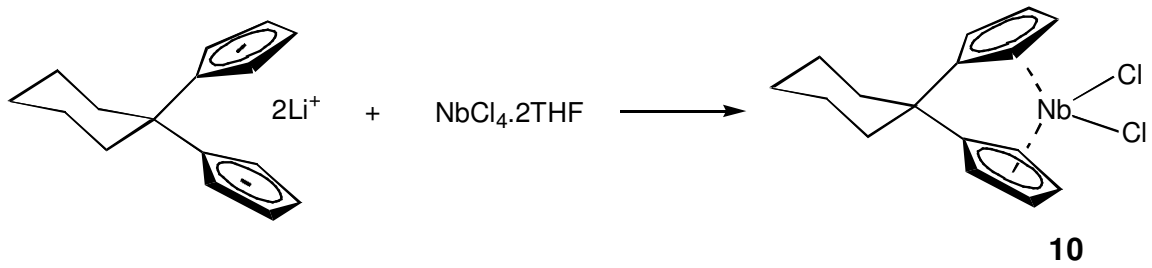

10

Scheme 2.11 Preparation of $[Nb\{(\eta-C_5H_4)C(C_5H_{10})(\eta-C_5H_4)\}Cl_2]$ **(10)**

Crude **10** was obtained as a dark brown solid in 70 % yield and was characterised by FAB mass spectrometry and ESR spectroscopy. An analytically pure sample of the compound **10** was obtained by sublimation at 160 °C (10^{-1}mmHg). The FAB mass spectrum of the compound **10** shows peaks due to the molecular ion and a fragment ion resulting from loss of a Cl ligand. The ESR spectrum consists of a 10 line pattern with a value of g_{iso} = 1.994 and a hyperfine splitting $|a^{93}Nb|_{iso}$ = 95 G. The isotropic coupling constant is typical for a single carbon bridged *ansa*-niobocene dichloride.

2.3.13 Preparation of $[Nb\{(\eta-C_5H_4)C(C_5H_{10})(\eta-C_5H_4)\}(\eta^2-BH_4)]$ (11)

The cyclohexyl-bridged tetrahydroborate derivative $[Nb\{(\eta-C_5H_4)C(C_5H_{10})(\eta-C_5H_4)\}(\eta^2-BH_4)]$ **(11)** was prepared by the action of lithium borohydride on the compound **10** in DME (**Scheme 2.12**). Extraction of the reaction mixture into light petroleum ether (b. p. 100-120 °C) and slow cooling to -80 °C afforded the compound **11** as a dark green crystalline solid.

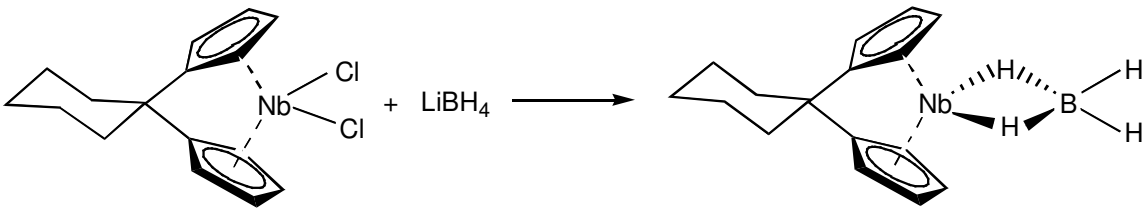

10 **11**

Scheme 2.12 Preparation of $[Nb\{(\eta-C_5H_4)C(C_5H_{10})(\eta-C_5H_4)\}(\eta^2-BH_4)]$ **(11)**

The compound **11** was characterised by IR specroscopy and ^1H, $^{13}C\{^1H\}$ and ^{11}B NMR spectroscopy. Elemental analyses were fully consistent with the proposed empirical

formula. The room temperature ^{1}H NMR spectrum of the compound **11** consists of two partial triplets at δ 5.70 and 4.61ppm corresponding to the two sets of protons of the cyclopentadienyl rings. The protons of the cyclohexyl bridge occur as three peaks; two peaks at δ 1.11 and 0.38 ppm due to the two sets of four protons closest to the bridgehead carbon, while the two protons furthest from the bridgehead carbon are located as a multiplet at δ 0.28 ppm. A broad resonance at δ -3.37 ppm corresponds to the protons of the BH_4 unit and implies that at room temperature bridge-terminal hydrogen exchange is fast on the NMR time scale, as for the compound **8** and [Nb(η–C_5H_5)$_2$(η^2–BH_4)].

In the ^{13}C{^{1}H} NMR spectrum peaks at δ 106.4 and 79.5 ppm correspond to the carbons of the cyclopentadienyl rings, with the *ipso*-carbon located at δ 81.3 ppm. Three peaks at δ 37.9, 30.2 and 26.2 ppm correspond to the nonbridging carbons of the cyclohexyl group with a peak at δ 30.6 ppm due to the bridgehead carbon. The ^{11}B NMR spectrum consists of a quintet ($^1J_{BH}$ = 90 Hz) at δ 18.2 ppm.

A variable temperature ^{1}H NMR study of the compound **11** allowed the calculation of the free energy barrier to bridge-terminal hydrogen exchange. Coalescence was observed at T_c = 218 ± 3 K corresponding to $\Delta G^{\ddagger}$ = 35.0 ± 1 kJ mol^{-1} in close agreement with the values of $\Delta G^{\ddagger}$ calculated for the compound **8** and [Nb(η–C_5H_4)CMe_2(η–C_5H_4)(η^2–BH_4)].

Single crystals of the compound **11** were obtained by slow cooling of a concentrated solution in petroleum ether (b. p. 100-120 ºC) to -80 ºC. However the crystals decomposed in the X-ray beam and the molecular structure was not determined. The first example of a structurally characterised cyclohexyl-bridged mononuclear *ansa*-metallocene, [W{(η–C_5H_4)$C(C_5H_{10})$(η–C_5H_4)}Me_2], is described in **Section 4.2.2**. The bridging unit is shown to influence the geometry of the metallocene in a manner typical for a single carbon *ansa*-bridge.

2.3.14 Preparation of [V{(η–C_5H_4)C_2Me_4(η–C_5H_4)}(η^2–BH_4)] (12)

The vanadocene tetrahydroborate complex [V(η–C_5H_5)$_2$(η^2–BH_4)] has been prepared and a free energy barrier to bridge-terminal hydrogen exchange of $\Delta G^{\ddagger}$ = 31.8 ± 2 kJ mol^{-1} reported.[8] Brintzinger has described the first entry into *ansa*-vanadocene chemistry *via* the dichloride complex [V{(η–C_5H_4)C_2Me_4(η–C_5H_4)}Cl_2], prepared by the reaction between VCl_3.THF and [$(MgCl)_2${$(C_5H_4)C_2Me_4(C_5H_4)$}.4THF] and subsequent

oxidation with PCl_3.[14] Reduction of $[V\{(\eta-C_5H_4)C_2Me_4(\eta-C_5H_4)\}Cl_2]$ with $LiAlH_4$ yields the monochloride $[V\{(\eta-C_5H_4)C_2Me_4(\eta-C_5H_4)\}Cl]$. From this V^{III} compound the cationic complexes $[V\{(\eta-C_5H_4)C_2Me_4(\eta-C_5H_4)\}L_2]^+$ (L = CO, ^{t}BuCN) are readily obtained *via* ligand exchange.

The compound $[V\{(\eta-C_5H_4)C_2Me_4(\eta-C_5H_4)\}(\eta^2-BH_4)]$ **(12)** was prepared by the reaction between $[V\{(\eta-C_5H_4)C_2Me_4(\eta-C_5H_4)\}Cl_2]$ and sodium borohydride at low temperature (**Scheme 2.13**). Extraction of the reaction mixture into petroleum ether (b. p. 100 - 120 °C) and slow cooling to -80 °C affords the compound **12** as an air- and moisture-sensitive violet crystalline solid.

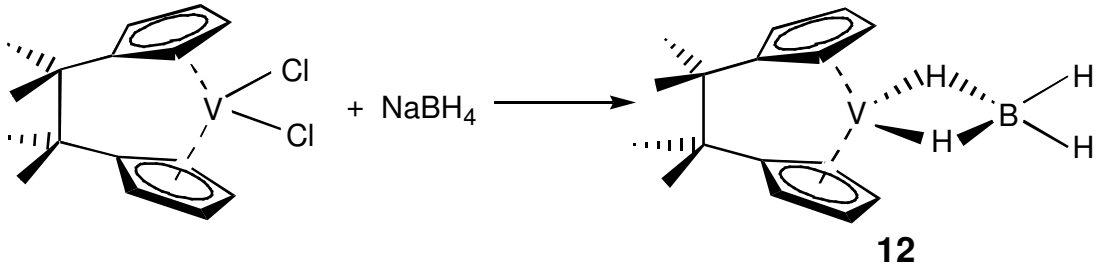

12

Scheme 2.13 Preparation of $[V\{(\eta-C_5H_4)C_2Me_4(\eta-C_5H_4)\}(\eta^2-BH_4)]$ **(12)**

The compound **12** was characterised by IR spectroscopy and ^1H, $^{13}C\{^1H\}$ and ^{11}B NMR spectroscopy. Elemental analyses were fully consistent with the proposed empirical formula. The IR spectra of the compound **12** shows two bands at 2450 and 2410 cm^{-1} assigned to the B-H_t symmetric and asymmetric stretches and two bands at 1750 and 1627 cm^{-1} assigned to the B-H_b symmetric and symmetric stretches. Bands were assigned by analogy to $[V(\eta-C_5H_5)_2(\eta^2-BH_4)]$[8] and the frequency of the B-H bond stretches observed in the IR spectrum of the compound **12** are comparable to the corresponding stretches in the analogous niobium compound **2**.

The ^1H, $^{13}C\{^1H\}$ and ^{11}B NMR spectra of the compound **12** are straightforward and essentially the same as that observed for the compound **2**. However, for the niobocene compound **2** to the protons of the BH_4 unit cannot be located in the room temperature ^1H NMR spectrum. In the case of the compound **12** a broad peak at δ -9.1 ppm corresponding the BH_4 protons implies that exchange is fast on the NMR time scale and that the free energy barrier to exchange $\Delta G^{\ddagger}$ is lower for the compound **12** compared

to the compound **2**. This is confirmed by a variable temperature ^{1}H NMR study of the compound **12**. Coalescence of terminal (δ 4.8 ppm) and bridging (δ -22.9 ppm) proton resonances is observed at $T_c = 263 \pm 3$ K, corresponding to $\Delta G^{\ddagger} = 41.5 \pm 1$ kJ mol^{-1}. For the corresponding niobium compound **2** $\Delta G^{\ddagger} = 49.1 \pm 1$ kJ mol^{-1}.

Slow cooling of a concentrated solution of the tetrahydroborate complex **12** in petroleum ether (b. p. 100-120 °C) to -80 °C afforded violet single crystals suitable for X-ray molecular structure determination. The crystal structure was determined and the molecular structure is shown in **Figure 2.11**. Selected interatomic distances and angles and other structural information are presented in **Table 2.5**. Full details of the molecular structure determination are given in **Appendix E**. The compound crystallises in the triclinic space group PI. Hydrogen atoms bound to boron were located in the final difference map and their positions refined.

The molecular structure of the compound **12** confirms the bidentate mode of bonding assigned by IR spectroscopy. The bending angle β is signficantly larger (*ca.* 5°) than the corresponding angle in the analogous niobium compound **2**. A decrease in bending angle β between first and second row bridged and nonbridged metallocenes has been reported for the compounds $[M(\eta\text{–}C_5H_5)_2Cl_2]$ (M = Ti, Zr) and $[M\{(\eta\text{–}C_5H_4)E(\eta\text{–}C_5H_4)\}Cl_2]$ (M = Ti, Zr; E = CMe_2, $SiMe_2$) (**Section 1.3**).[28] As for the other ethylene-bridged compounds **2** and *rac*-**5**, there is a small departure in planarity at the *ipso*-carbons (ϕ *ca* -1.8°). Again the *ipso*-carbon vector lies above the plane of the cyclopentadienyl rings reflecting the steric demand of a two-carbon bridge. In the compound **12** the *ipso*-carbons and the carbons of the bridge are not coplanar, corresponding to a twisting of the bridging unit.

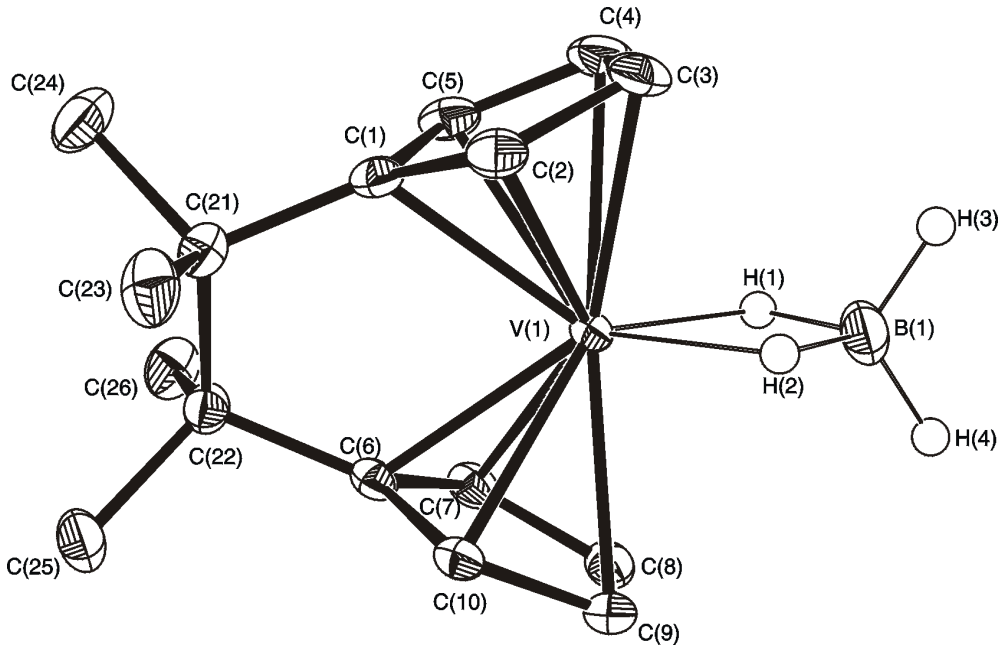

Figure 2.11 Molecular structure of $[V\{(\eta-C_5H_4)C_2Me_4(\eta-C_5H_4)\}(\eta^2-BH_4)]$ **(12).** Hydrogen atoms attached to carbon atoms are omitted for clarity.

	Length / Å		Angle / °
V-Cp^1_{cent}	1.9050	Between Cp planes, α	47.7
V-Cp^1_{ave}	2.2552(17)	Cp^1_{norm}-V-Cp^2_{norm}, β	132.3
V-Cp^2_{cent}	1.9029	Cp^1_{cent}-V-Cp^2_{cent}, χ	137.71
V-Cp^2_{ave}	2.2530(17)	C_{ipso}-Cp plane, ϕ	-2.0, -1.6
V-C(1)	2.2159(15)		
V-C(3)	2.2861(18)		
C_{ipso}-C_{ipso}	2.5996		
V-H(1)	1.76(3)		
B-H(1)	1.18(3)		
B-H(3)	1.06(3)		

Cp^1 = Ring C(1)-C(5), Cp^2 = Ring C(6)-C(10)

Table 2.5 Selected interatomic distances and angles and other structural information for $[V\{(\eta-C_5H_4)C_2Me_4(\eta-C_5H_4)\}(\eta^2-BH_4)]$ **(12)**

2.4 Attempted Investigation of the Mechanism of Bridge-Terminal Hydrogen Exchange

2.4.1 Synthesis of a Mixed-Ring *ansa*-Metallocene

In order to further study the mechanism of bridge-terminal hydrogen exchange in Group 5 *ansa*-metallocene tetrahydroborate complexes it was decided to prepare a mixed-ring *ansa*-metallocene. Principally it was hoped to use quantitative phase-sensitive 2D exchange (EXSY) ^{1}H NMR spectroscopy to elucidate rate constants for exchange between the four hydrogens of the tetrahydroborate unit. Green and Wong have shown for the compound $[Ta(\eta\text{–}C_5H_5)(\eta\text{–}C_5Me_5)(\eta^2\text{–}BH_4)]$ that there is negligible direct exchange between the terminal hydrogens of the BH_4 unit.[13] Thus an associative mechanism involving coordination of a terminal hydrogen in an η^3-BH_4 unit was proposed (**Section 2.2**). The purpose of the mixed-ring system was to allow differentiation of the terminal B-H hydrogens.

The free energy barrier to bridge-terminal hydrogen exchange $\Delta G^{\ddagger}$ must be sufficiently large so that access to sharp distinct resonances for the terminal B-H hydrogens in the slow exchange limit is possible. Therefore a single carbon-bridged mixed ring *ansa*-metallocene system was ruled out since peaks due to terminal B-H hydrogens are prohibitively broad even at 183 K as $\Delta G^{\ddagger}$ for the exchange process is relatively small. Rather it was decided to prepare the silicon-bridged mixed *ansa*-metallocene tetrahydroborate complex $[Nb\{(\eta\text{–}C_5H_3Me)SiMe_2(\eta\text{–}C_5H_4)\}(\eta^2\text{–}BH_4)]$. It was anticipated that this ring system would render the four tetrahydroborate hydrogens inequivalent in the slow exchange limit and that $\Delta G^{\ddagger}$ for the exchange process would be sufficiently large to give sharp peaks in the low temperature ^{1}H NMR spectrum.

2.4.2 Preparation of $[Li_2\{(C_5H_3Me)SiMe_2(C_5H_4)\}]$

The synthesis of *ansa*-bridged mixed-ring systems with a view to preparing chiral C_s symmetric metallocenes for the stereospecific polymerisation of olefins has been extensively reported in recent years. Ewen described the production of highly syndiotactic polypropene using $[M\{(\eta\text{–}C_5H_4)CMe_2(\eta\text{–}C_{13}H_8)\}Cl_2]$ (M = Zr, Hf) and the co-catalyst MAO over a wide range of polymerisation temperatures.[32] Green reported that the analogous cyclopentadienyl/indenyl system $[M\{(\eta\text{–}C_5H_4)CR_2(\eta\text{–}C_9H_6)\}Cl_2]$ (M = Ti, Zr,

Hf; CR_2 = CMe_2, CPh_2) with MAO and the appropriate olefin yields isotactic rich polypropene and polystyrene.[33]

The mixed-ring ligand $[Li_2\{(C_5H_3Me)SiMe_2(C_5H_4)\}]$ was prepared in an analogous procedure to that employed in the synthesis of $[Li_2\{(C_5H_4)SiMe_2(C_{13}H_8)\}]$ (**Scheme 2.14**).[34] A solution of one equivalent of $[Li(C_5H_4Me)]$ in THF was added to a solution of Me_2SiCl_2 in diethyl ether. The compound $[(C_5H_4Me)SiMe_2Cl]$ **(13)** was collected as a pale yellow extremely moisture sensitive oil following distillation at 125 °C (10^{-1}mmHg).

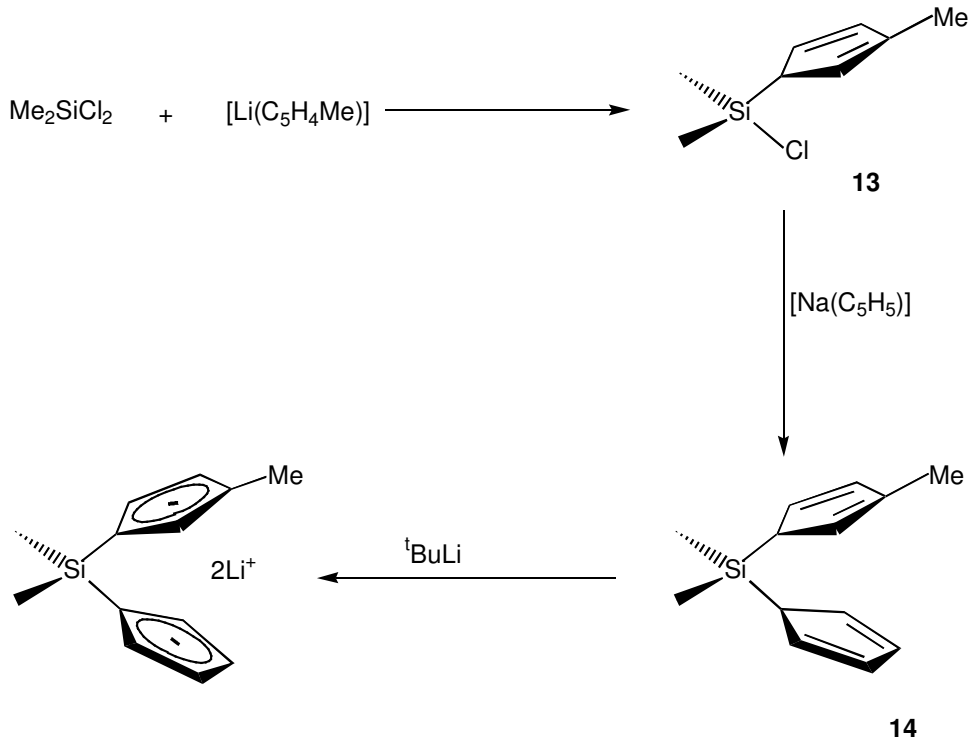

Scheme 2.14 Preparation of $[Li_2\{(C_5H_3Me)SiMe_2(C_5H_4)\}]$

The compound **13** was characterised by ^1H and $^{13}C\{^1H\}$ NMR spectroscopy. The ^1H NMR spectrum of **13** in CD_2Cl_2 consists of four singlets at δ 6.56, 6.49, 6.12 and 3.55 ppm corresponding to the four protons of methylcyclopentadienyl ring. A singlet at δ 2.06 ppm is assigned to the protons of the methyl group attached to the ring. The protons of the $SiMe_2$ bridge are located as a pair of singlets at δ 0.27 and 0.22 ppm. In the $^{13}C\{^1H\}$ NMR spectrum four peaks at δ 146.1, 138.8, 135.6 and 129.2 ppm are assigned to the ring carbons with the *ipso*-carbon located at δ 55.1 ppm. A singlet at δ 17.8 ppm corresponds to the methyl carbon attached to the ring. The methyl carbons of the $SiMe_2$ bridge are assigned to a pair of singlets at δ 3.1 and 2.6 ppm. The extremely moisture-

sensitive nature of the compound **13** precluded characterisation by elemental analysis or gas-chromotography-mass spectrometry.

Addition of sodium cyclopentadienide to a solution of the compound $[(C_5H_4Me)SiMe_2Cl]$ **(13)** in diethyl ether (100 cm^3) containing 10 % TMEDA gives an orange solution. Following hydrolysis with a saturated aqueous solution of NH_4Cl, separation of the organic layer prior to drying over anhydrous $MgSO_4$ and removal of volatiles, the compound $[(C_5H_4Me)SiMe_2(C_5H_5)]$ **(14)** was obtained as an orange oil.

The compound **14** was characterised by ^1H NMR spectroscopy. The ^1H NMR spectrum consists of a broad multiplet resonance at δ 6.63-6.60 ppm corresponding to seven protons and assigned to seven of the nine protons of the cyclopentadienyl and methylcyclopentadienyl rings. The remaining ring protons are located as a pair of singlets at δ 2.96 and 2.85 ppm. Singlets at δ 2.06, -0.29 and –0.31 ppm are assigned to the protons of ring methyl group and the methyl protons of the $SiMe_2$ bridge respectively.

The neutral ligand **14** was deprotonated by the cautious addition of a solution of ^tBuLi in pentane to a solution of **14** in light petroleum ether (b.p. 40 – 60 ºC). The compound $[Li_2(C_5H_3Me)SiMe_2(C_5H_4)]$ was isolated as an air-sensitive pale yellow solid and used without characterisation.

2.4.3 Preparation of $[Nb\{(\eta\text{–}C_5H_3Me)SiMe_2(\eta\text{–}C_5H_4)\}Cl_2]$ (15)

The mixed-ring *ansa*-metallocene compound $[Nb\{(\eta\text{–}C_5H_3Me)SiMe_2(\eta\text{–}C_5H_4)\}Cl_2]$ **(15)** was prepared by the reaction between $NbCl_4.2THF$ and $[Li_2\{(C_5H_3Me)SiMe_2(C_5H_4)\}]$ in an analogous procedure to that used to prepare the compound **1** (**Scheme 2.15).**

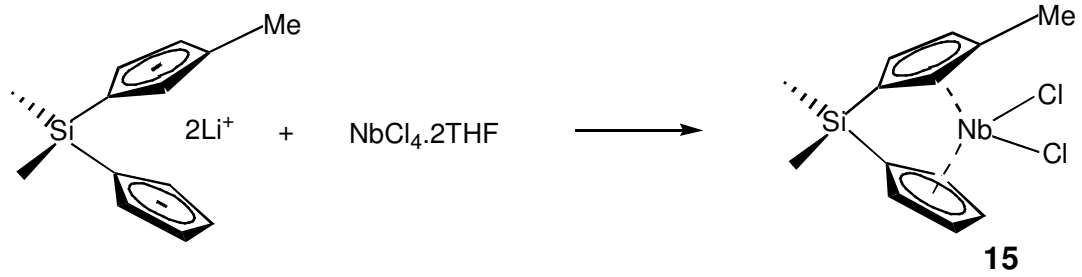

Scheme 2.15 Preparation of $[Nb\{(\eta\text{–}C_5H_3Me)SiMe_2(\eta\text{–}C_5H_4)\}Cl_2]$ **(15)**

The compound **15** was characterised by FAB mass spectrometry and ESR spectroscopy. The FAB mass spectrum of the compound **15** shows fragment peaks due to the consecutive loss of one and two Cl ligands. The parent ion was not located. The ESR spectrum shows the expected 10 line pattern with g_{iso} = 2.007 and an isotropic coupling constant $|a^{93}Nb|_{iso}$ = 109 G. As expected the value for the isotropic coupling constant is very similar to that obtained for the ethylene-bridged compound **2** ($|a^{93}Nb|_{iso}$ = 110 G). The influence of a silicon- and ethylene-bridge is again shown to be similar.

2.4.4 Preparation of [Nb{(η–C_5H_3Me)$SiMe_2$(η–C_5H_4)}(η^2–BH_4)] (16)

The silicon-bridged mixed-ring tetrahydroborate derivative [Nb{(η–C_5H_3Me)$SiMe_2$(η–C_5H_4)}(η^2–BH_4)] **(16)** was prepared by the action of lithium borohydride on a suspension of the compound **15** in DME (**Scheme 2.16**). The compound **16** was extracted from the reaction mixture into petroleum ether (b. p. 100 - 120 °) to give an oily green solid. An analytically pure sample of the compound **16** was obtained by sublimation at 70 °C (10^{-1} mm Hg).

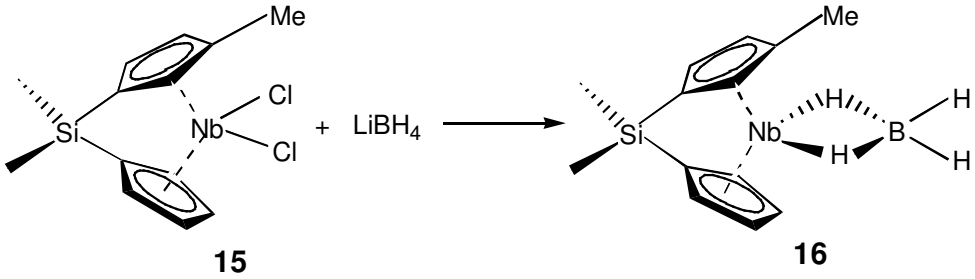

Scheme 2.16 Preparation of [Nb{(η–C_5H_3Me)$SiMe_2$(η–C_5H_4)}(η^2–BH_4)] **(16)**

The tetrahydroborate compound **16** was fully characterised by elemental analysis, IR spectroscopy, ^1H, $^{13}C\{^1H\}$ and ^{11}B NMR spectroscopy and FAB mass spectrometry. The IR spectrum shows the expected pair of B-H_t stretches at 2468 and 2423 cm^{-1} and pair of B-H_b stretches at 1700 and 1649 cm^{-1}. The ^1H NMR spectrum of the compound **16** consists of seven singlets at δ 6.04, 5.89, 5.74, 5.36, 5.27, 5.17 and 4.95 ppm corresponding to the seven inequivalent protons of the cyclopentadienyl rings. The ring methyl protons occur as a singlet at δ 1.95 ppm. Two singlets at δ -0.72 and –0.79 ppm are assigned to the protons of the $SiMe_2$ bridging unit.

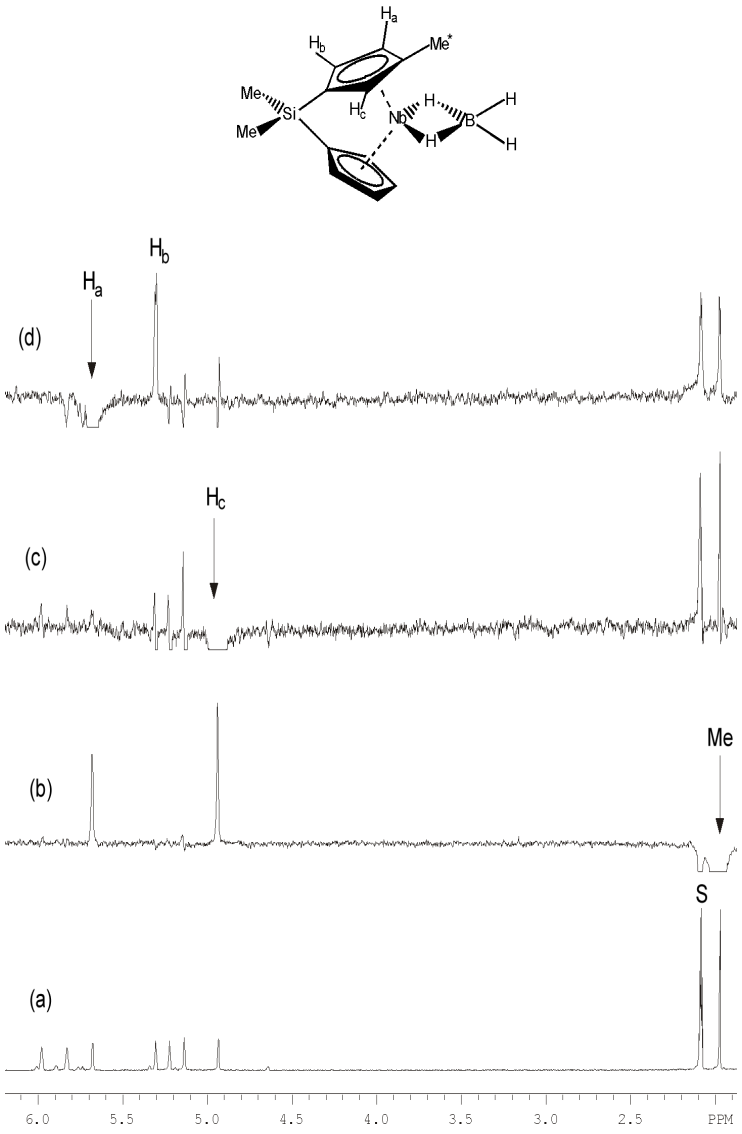

Figure 2.12 ^{1}H NMR NOE difference spectra of the compound $[Nb\{(\eta-C_5H_3Me)SiMe_2(\eta-C_5H_4)\}(\eta^2-BH_4)]$ **(16).** S denotes a residual solvent peak.

There are two possible positions for the methyl group attached to one of the cyclopentadienyl rings i.e. adjacent to the *ipso*-carbon or two ring carbon atoms from it. In order to unambiguously confirm the structure of the compound **16** and assign the peaks in the ^{1}H NMR spectrum, a series of NOE difference experiments were performed (**Figure 2.12**). Spectrum (a) is the normal ^{1}H NMR spectrum in the region δ 6.2 – 1.8 ppm. In spectrum (b) irradiation of the methyl resonance at δ 1.95 ppm results in NOE enhancements at δ 5.74 and 4.95 ppm which are thus assigned to the a and c positions.

Irradiation of the H_c resonance at δ 4.95 ppm shows in spectrum (c) a significant NOE enhancement at δ 1.95 ppm only corresponding to the ring methyl protons. Finally in spectrum (d), irradiation of the H_a resonance at δ 5.74 ppm shows NOE enhancements at δ 5.36 and 1.95 ppm corresponding to H_b and the ring methyl protons. The remaining resonances in the Cp region at δ 6.04, 5.89, 5.27 and 5.17 ppm are thus assigned to the four inequivalent protons of the nonmethylated cyclopentadienyl ring.

The $^{13}C\{^1H\}$ NMR spectrum was fully assigned using a $^1H\{^{13}C\}$ HMQC experiment and is not discussed here. The ^{11}B spectrum shows a quintet ($^1J_{BH}$ = 88 Hz) centred at δ 22.0 ppm.

A variable temperature ^1H NMR study of the compound **16** allowed elucidation of the free energy barrier to exchange $\Delta G^{\ddagger}$ at the coalescence temperature. At high temperature (*ca*. 363 K) exchange is fast on the NMR time scale and a single broad resonance is observed at δ -4.8 ppm. As the temperature is decreased this resonance broadens until coalescence occurs at $T_c = 302 \pm 3$ K, corresponding to $\Delta G^{\ddagger} = 48.8 \pm 1$ kJ mol^{-1}. For the analogous silicon-bridged compound **6** $\Delta G^{\ddagger} = 49.3 \pm 1$ kJ mol^{-1}. As seen in **Figure 2.13** as the temperature is reduced below the coalescence temperature the peak due to the bridging hydrogens at δ -14.9 ppm starts to split into two resonances. These two resonances correspond to the bridging hydrogens which are in inequivalent environments. The peak due to the terminal hydrogens at δ 5.3 ppm is obscured by the peaks due to the cyclopentadienyl protons although it does appear to be broader than that for the bridging hydrogens.

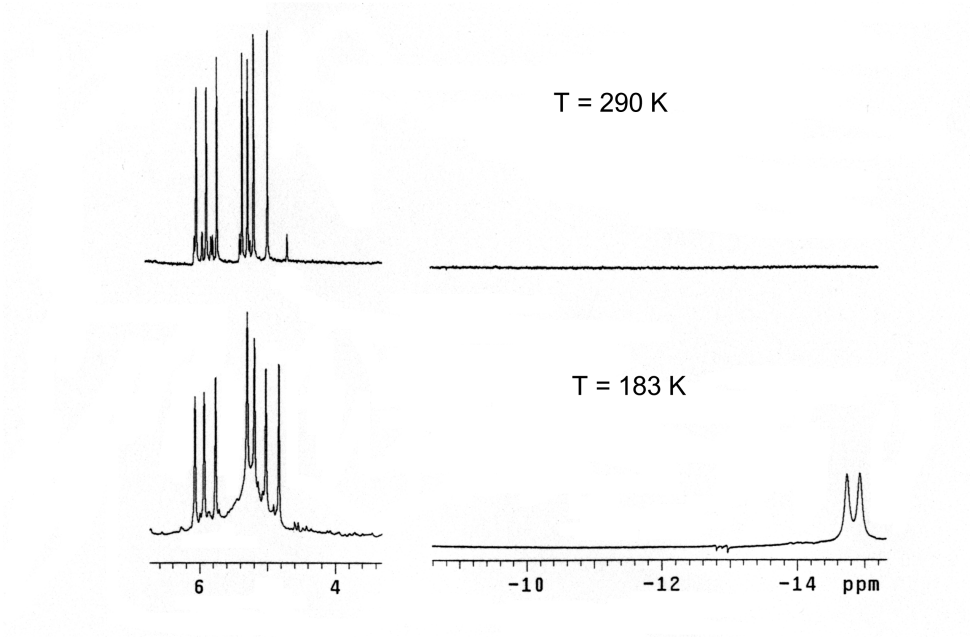

Figure 2.13 Partial variable temperature ^{1}H NMR spectra of the compound $[Nb\{(\eta-C_5H_3Me)SiMe_2(\eta-C_5H_4)\}(\eta^2-BH_4)]$ **(16)**

The broadness of the peak due to the terminal hydrogens presented a problem for the proposed EXSY experiment. A ^{1}H NMR EXSY ($C_6D_5CD_3$) experiment was carried out on the compound **16** at 183 K. As was feared a cross peak between inequivalent terminal hydrogens was not observed due to the broadness of the resonance. ^{11}B decoupling did not reduce the broadness of the resonance sufficiently to allow observation of inequivalent hydrogens. Cross peaks between the inequivalent bridging hydrogens and between the bridging hydrogens and the terminal hydrogens were observed. A solution to the problem would be to perform the experiment at temperatures below 183 K in a low freezing point solvent such as $CDCl_2F$. Such attempts were precluded by the reactivity of this solvent towards the compound **16** and thus quantitative determination of the rate constants for exchange between all hydrogens of the tetrahydroborate unit was prevented.

2.4.5 Preparation of $[Nb\{(\eta-C_5H_3Me)SiMe_2(\eta-C_5H_4)\}(\eta^2-BD_4)]$ (17)

The isotopically substituted compound $[Nb\{(\eta-C_5H_3Me)SiMe_2(\eta-C_5H_4)\}(\eta^2-BD_4)]$ **(17)** was prepared by the reaction between the compound **15** and sodium borodeuteride. The compound **17** was extracted from the

reaction mixture into petroleum ether (b. p. 100 - 120 °C) to give an green oily solid. An analytically pure sample of the compound **17** was obtained by sublimation at 70 °C (10^{-1}mm Hg).

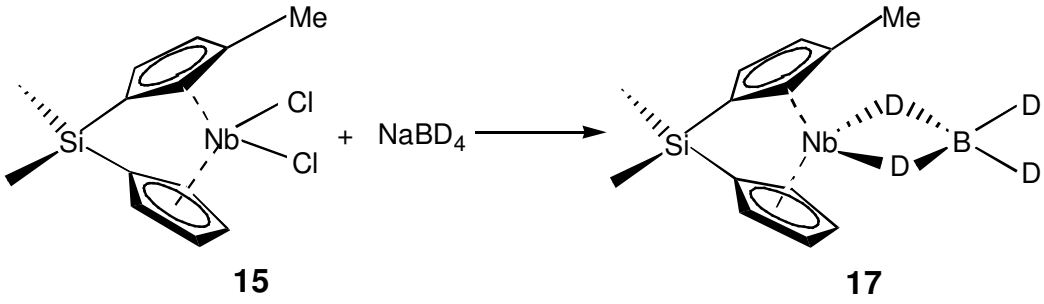

Scheme 2.17 Preparation of [Nb{(η–C_5H_3Me)$SiMe_2$(η–C_5H_4)}(η^2–BD_4)] **(17)**

The compound **17** was fully characterised and characterisation is not discussed further here. The free energy barrier to bridge-terminal hydrogen exchange was found to be $\Delta G^{\ddagger}$ = 48.7 ± 1 kJ mol^{-1}. As expected $\Delta G^{\ddagger}$ is comparable to that found for the compound **16** ($\Delta G^{\ddagger}$ = 48.8 ± 1 kJ mol^{-1}). **Figure 2.14** shows the ^{2}H NMR ($C_6H_5CD_3$) spectrum of the compound **17** at 193 K. It can be seen that the peak due to the inequivalent terminal hydrogens at δ 4.9 ppm has not yet begun to separate into the expected pair of resonances.

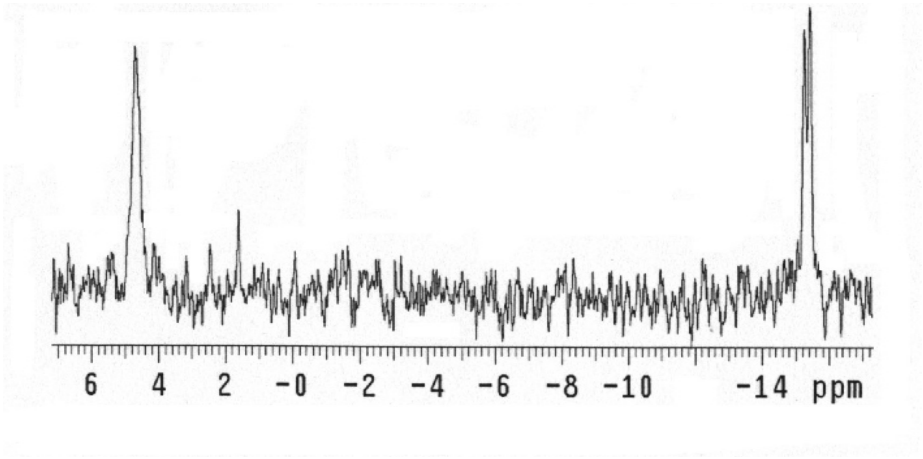

Figure 2.14 ^{2}H NMR spectrum of the compound [Nb{(η–C_5H_3Me)$SiMe_2$(η–C_5H_4)}(η^2–BD_4)] **(16)** at 193 K

2.5 Comparison of Group 5 Metallocene Tetrahydroborate Complexes

2.5.1 Comparison of Structural Properties

A comparison of structural features of the new Group 5 *ansa*-metallocene tetrahydroborate complexes described in this chapter holds few surprises. Relevant structural parameters of the compounds **2**, *rac*-**5**, **6**, **8** and **12** are compared to the corresponding nonbridged compounds in **Table 2.6**. As expected the greatest influence on the structure is exerted by a single-carbon bridge. The angle between the rings α is increased in the presence of such a bridging unit and thus the corresponding bending angle β is reduced. The magnitude of this reduction in β is large with β *ca.* 13° smaller in the compound **8** than the analogous nonbridged compound $[Nb(\eta-C_5H_5)_2(\eta^2-BH_4)]$. There is a large deviation from planarity at the *ipso*-carbon atoms with an average value of ϕ *ca.* 20° for the silicon bridged-compound **6** and ϕ *ca.* 17° for the single carbon-bridged compounds **8** and $[Nb\{(\eta-C_5H_4)CMe_2(\eta-C_5H_4)\}(\eta^2-BH_4)]$.

Compound	α / °	β / °	γ / °	ϕ/ °[b]	C_{ipso}-C_{ipso} (Å)	Ref.
$[Nb(\eta-C_5H_5)_2(\eta^2-BH_4)]$	50.2	129.8	130.0			26, 27
$[Nb\{(\eta-C_5Me_5)_2\ (\eta^2-BH_4)]$	40.8	139.2	146.0			26, 35
$[Nb\{(\eta-C_5H_4)C_2Me_4(\eta-C_5H_4)\}(\eta^2-BH_4)]$ **(2)**	52.2	127.8	134.8	-2.5	2.685	*a*
rac-$[Nb\{(\eta-C_5H_3$-^{t}Bu$)C_2Me_4(\eta-C_5H_3$-^{t}Bu$)\}$ $(\eta^2-BH_4)]$ **(5)**	55.3	124.7	133.6	-4.1	2.664	*a*
$[Nb\{(\eta-C_5H_4)SiMe_2(\eta-C_5H_4)\}(\eta^2-BH_4)]$ **(6)**	52.8	127.2	135.7	20.6	2.699	*a*
$[Nb\{(\eta-C_5H_4)CMe_2(\eta-C_5H_4)\}(\eta^2-BH_4)]$	65.9	114.1	125.0	17.0	2.266	*a,* 10
$[Nb\{(\eta-C_5H_4)CEt_2(\eta-C_5H_4)\}(\eta^2-BH_4)]$ **(8)**	64.4	115.6	125.0	17.2	2.293	*a*
$[V\{(\eta-C_5H_4)C_2Me_4(\eta-C_5H_4)\}(\eta^2-BH_4)]$ **(12)**	47.7	132.3	137.7	-1.8	2.5996	*a*

[a] This work [b] Average value of ϕ

Table 2.6 Selected structural features of Group 5 metallocene tetrahydroborate complexes

The structural consequences of the introduction of an *ansa*-bridge on the metallocene geometry are considerably less marked for the ethylene-bridged compounds **2**

and *rac*-**5** and the silicon-bridged compound **6**. The inter-ring angle α and hence the bending angle β are closely similar to those found for the nonbridged tetrahydroborate complex. As found in related systems, the introduction of an ethylene-bridge has a similar structural effect as a silicon-bridge (**Section 1.3**). The principal difference in the effect imparted by these bridging units is the inherent strain at the *ipso*-carbon imposed by a single-atom bridge, as in the silicon bridged compound **6**, compared to a two-atom bridge. Rather unexpectedly the angle ϕ is larger for the compound **6** than the methylene-bridged compound **8**.

Comparison of relevant structural parameters for the analogous tetramethyethylene-bridged compounds **12** and **2** shows the expected change in ring angles on moving from a first row to a second row transition metal. The bending angle β in the vanadocene compound **12**, with its smaller metal centre, is larger than in the corresponding niobocene compound **2**.

2.5.2 Comparison of B-H IR Stretching Frequencies

In the molecular structures determined the bridging B-H_b bond lengths are greater than the terminal B-H_t bond lengths, consistent with a covalent interaction between the metal and BH_4 ligand. This is also reflected in the B-H stretching frequencies with the terminal B-H stretching frequencies found at higher energy than the bridging B-H stretching frequencies. B-H stretching frequencies for Group 5 metallocene tetrahydroborate complexes are presented in **Table 2.7**.

Compound	$\nu(B\text{-}H_t)/cm^{-1}$	$\nu(B\text{-}H_b)/cm^{-1}$	Ref.
$[Nb(\eta\text{–}C_5H_5)_2(\eta^2\text{–}BH_4)]$	2460, 2423	1745, 1650	1
$[Nb(\eta\text{–}C_5Me_5)_2(\eta^2\text{–}BH_4)]$	2452, 2428	1728, 1620	26
$[Nb\{(\eta\text{–}C_5H_4)C_2Me_4(\eta\text{–}C_5H_4)\}(\eta^2\text{–}BH_4)]$ **(2)**	2465, 2427	1712, 1661	*a*
rac-$[Nb\{(\eta\text{–}C_5H_3\text{-}^tBu)C_2Me_4(\eta\text{–}C_5H_3\text{-}^tBu)\}(\eta^2\text{–}BH_4)]$ **(5)**	2467, 2430	1690, 1666	*a*
$[Nb\{(\eta\text{–}C_5H_4)SiMe_2(\eta\text{–}C_5H_4)\}(\eta^2\text{–}BH_4)]$ **(6)**	2460, 2410	1703, 1652	*a*
$[Nb\{(\eta\text{–}C_5H_3Me)SiMe_2(\eta\text{–}C_5H_4)\}(\eta\text{–}BH_4)]$ **(16)**	2468, 2423	1700, 1649	*a*
$[Nb\{(\eta\text{–}C_5H_4)CEt_2(\eta\text{–}C_5H_4)\}(\eta^2\text{–}BH_4)]$ **(8)**	2442, 2395	1715, 1703	*a*
$[Nb\{(\eta\text{–}C_5H_4)C(C_5H_{10})(\eta\text{–}C_5H_4)\}(\eta^2\text{–}BH_4)]$ **(11)**	2417, 2402	1705, 1695	*a*
$[V(\eta\text{–}C_5H_5)_2(\eta^2\text{–}BH_4)]$	2442, 2418	1745, 1650	8
$[V\{(\eta\text{–}C_5H_4)C_2Me_4(\eta\text{–}C_5H_4)\}(\eta^2\text{–}BH_4)]$ **(12)**	2450, 2410	1750, 1627	*a*

[a] This work

Table 2.7 Selected IR stretching frequencies for Group 5 metallocene tetrahydroborate complexes

Girolami has described the use of the correlation between the average symmetric and asymmetric stretching frequencies for the B-H_t and B-H_b bonds as a gauge of the M-BH_4 covalent interaction.[36] **Figure 2.15** shows these parameters for the compounds **2**, *rac*-**5**, **6**, **8**, **11**, **12** and **16** and for the non-bridged species $[Nb(\eta\text{–}C_5H_5)_2(\eta^2\text{–}BH_4)]$, $[Nb(\eta\text{–}C_5Me_5)_2(\eta^2\text{–}BH_4)]$ and $[V(\eta\text{–}C_5H_5)_2(\eta^2\text{–}BH_4)]$. Although the comparison is somewhat crude it can seen that there is a slight strengthening of the B-H_b bonds and weakening of the B-H_t bonds in the methylene-bridged species **8** and **11** relative to the non-bridged analogues, suggesting a reduced M-BH_4 covalent interaction. The average stretching frequencies for the silicon- and ethylene-bridged compounds are more similar to the parent nonbridged metallocenes. Theoretical studies on *ansa*-metallocenes show that as the bending angle β is reduced, two of the metal d-orbitals become more involved in metal-ring bonding and are less available for binding other ligands (**Section 4.2.7**).[31, 37] Density functional calculations also show that as the *ansa*-bridge becomes more

constraining, as evidenced by an increased inter-ring angle α and a reduced bending angle β, the tetrahydroborate unit becomes more weakly bound (**Section 2.6**).

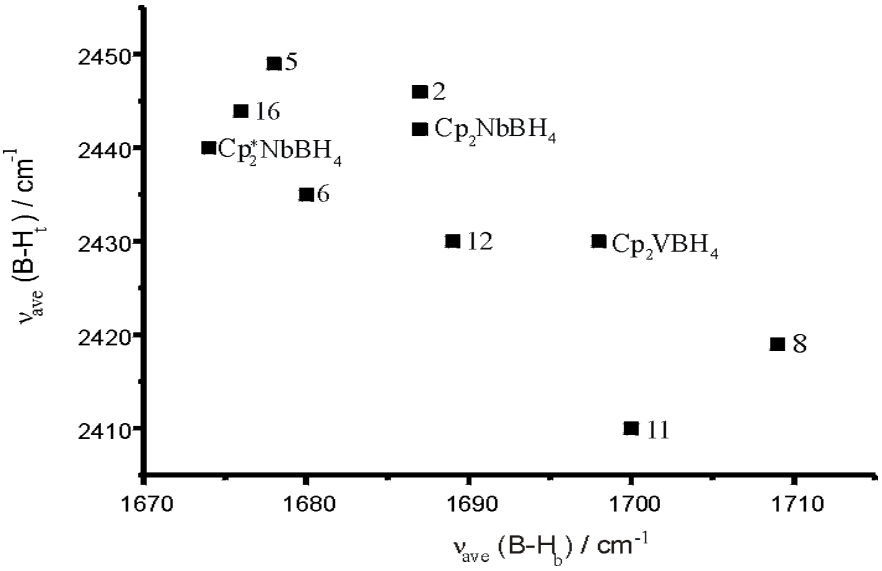

Figure 2.15 Average B-H stretching frequencies for Group 5 metallocene tetrahydroborate complexes

2.5.3 Comparison of Dynamic Properties

As has been described above, the hydrogen exchange processes for a series of new Group 5 *ansa*-metallocene tetrahydroborate complexes has been studied using variable temperature NMR spectroscopy. The relevant spectral data for these compounds and analogous nonbridged compounds are summarised in **Table 2.8**.

Compound	T_c / K	δ_t / ppm	δ_b / ppm	$\delta_{b/t}$ / ppm	Ref.
$[Nb(\eta-C_5H_5)_2(\eta^2-BH_4)]$	346 ± 3^c	5.1	-16.2	-5.4	26
$[Nb(\eta-C_5Me_5)_2(\eta^2-BH_4)]$	388 ± 8^c	5.2	-18.2	-7.0	26
$[Nb\{(\eta-C_5H_4)C_2Me_4(\eta-C_5H_4)\}(\eta^2-BH_4)]$ **(2)**	308 ± 3^a	5.3	-14.9	-5.0	*b*
$[Nb\{(\eta-C_5H_4)C_2Me_4(\eta-C_5H_4)\}(\eta^2-BD_4)]$ **(3)**	278 ± 5^d	4.9	-15.3	-4.9	*b*
rac-$[Nb\{(\eta-C_5H_3$-^{t}Bu$)C_2Me_4(\eta-C_5H_3$-^{t}Bu$)\}(\eta^2-BH_4)]$ **(5)**	303 ± 3^a	5.2	-13.9	-4.5	*b*
$[Nb\{(\eta-C_5H_4)SiMe_2(\eta-C_5H_4)\}(\eta^2-BH_4)]$ **(6)**	305 ± 3^a	5.5	-14.9	-5.0	*b*
$[Nb\{(\eta-C_5H_3Me)SiMe_2(\eta-C_5H_4)\}(\eta^2-BH_4)]$ **(16)**	302 ± 3^a	5.3	-14.8	-4.8	*b*
$[Nb\{(\eta-C_5H_3Me)SiMe_2(\eta-C_5H_4)\}(\eta^2-BD_4)]$ **(17)**	276 ± 5^d	4.9	-15.2	-4.6	*b*
$[Nb\{(\eta-C_5H_4)CMe_2(\eta-C_5H_4)\}(\eta^2-BH_4)]$	228 ± 3^a	5.2	-11.6	-3.4	*b*
$[Nb\{(\eta-C_5H_4)CMe_2(\eta-C_5H_4)\}(\eta^2-BD_4)]$ **(9)**	198 ± 5^d	4.2	-12.3	-3.0	*b*
$[Nb\{(\eta-C_5H_4)CEt_2(\eta-C_5H_4)\}(\eta^2-BH_4)]$ **(8)**	223 ± 3^a	5.3	-11.6	-3.5	*b*
$[Nb\{(\eta-C_5H_4)C(C_5H_{10})(\eta-C_5H_4)\}(\eta^2-BH_4)]$**(11)**	218 ± 3^a	5.3	-11.5	-3.4	*b*
$[V(\eta-C_5H_5)_2(\eta^2-BH_4)]$	186 ± 7^c	5.0	-24.0	-9.5	8
$[V\{(\eta-C_5H_4)C_2Me_4(\eta-C_5H_4)\}(\eta^2-BH_4)]$ **(12)**	263 ± 3^a	4.8	-22.9	-9.1	*b*

[a] 500 MHz, [b] This work, [c] 90 MHz, [d] 76 MHz

Table 2.8 Variable temperature ^{1}H NMR spectroscopy data for Group 5 metallocene tetrahydroborate complexes

The free energy barrier to bridge-terminal hydrogen exchange $\Delta G^{\ddagger}$, the inter-ring angle α and the bending angle β for Group 5 metallocene tetrahydroborate complexes are compared in **Table 2.9**. In order to make a meaningful comparison between the values of $\Delta G^{\ddagger}$ for the various tetrahydroborate complexes it is assumed that $\Delta S^{\ddagger}$ for the exchange process is essentially the same for all species. Furthermore it is assumed that exchange proceeds *via* the same mechanism in all cases.

The presence of an *ansa*-bridge reduces $\Delta G^{\ddagger}$ for the bridge-terminal hydrogen exchange process for the niobocene complexes. The effect is most marked when the *ansa*-bridge exerts the greatest change in the geometry of the metallocene unit, i.e. the reduction

in the bending angle β is greatest. Thus for the methylene-bridged compound **8** the bending angle is reduced by 14.2° compared to the nonbridged compound and the free energy barrier $\Delta G^{\ddagger}$ is *ca.* 25 kJ mol^{-1} smaller. The effect of the introduction of an ethylene- or silicon-bridge is less significant, with $\Delta G^{\ddagger}$ reduced by around 10 kJ mol^{-1}. As described in **Section 2.5.1** such a bridge imparts little change in the orientation of the rings relative to the metal. Again it is noted that the '*ansa*-effect' exerted by an ethylene- or silicon-bridge is similar.

Compound	$\Delta G^{\ddagger}$ / kJ mol^{-1}	α / °	β / °	Ref.
$[Nb(\eta\text{–}C_5H_5)_2(\eta^2\text{–}BH_4)]$	61.1 ± 1	50.2	129.8	26, 27
$[Nb(\eta\text{–}C_5Me_5)_2(\eta^2\text{–}BH_4)]$	68.6 ± 2	40.8	139.2	26, 35
$[Nb\{(\eta\text{–}C_5H_4)C_2Me_4(\eta\text{–}C_5H_4)\}(\eta^2\text{–}BH_4)]$ **(2)**	49.9 ± 1	52.2	127.8	*a*
$[Nb\{(\eta\text{–}C_5H_4)C_2Me_4(\eta\text{–}C_5H_4)\}(\eta^2\text{–}BD_4)]$ **(3)**	49.1 ± 2			*a*
rac-$[Nb\{(\eta\text{–}C_5H_3\text{-}^t Bu)C_2Me_4(\eta\text{–}C_5H_3\text{-}^t Bu)\}(\eta^2\text{–}BH_4)]$ **(5)**	49.1 ± 1	55.3	124.7	*a*
$[Nb\{(\eta\text{–}C_5H_4)SiMe_2(\eta\text{–}C_5H_4)\}(\eta^2\text{–}BH_4)]$ **(6)**	49.3 ± 1	52.8	127.2	*a*
$[Nb\{(\eta\text{–}C_5H_3Me)SiMe_2(\eta\text{–}C_5H_4)\}(\eta^2\text{–}BH_4)]$ **(16)**	48.8 ± 1			*a*
$[Nb\{(\eta\text{–}C_5H_3Me)SiMe_2(\eta\text{–}C_5H_4)\}(\eta^2\text{–}BD_4)]$ **(17)**	48.7 ± 2			*a*
$[Nb\{(\eta\text{–}C_5H_4)CMe_2(\eta\text{–}C_5H_4)\}(\eta^2\text{–}BH_4)]$	35.0 ± 1	65.9	114.1	*a,* 10
$[Nb\{(\eta\text{–}C_5H_4)CMe_2(\eta\text{–}C_5H_4)\}(\eta^2\text{–}BD_4)]$ **(9)**	34.8 ± 2			*a*
$[Nb\{(\eta\text{–}C_5H_4)CEt_2(\eta\text{–}C_5H_4)\}(\eta^2\text{–}BH_4)]$ **(8)**	35.8 ± 1	64.4	115.6	*a*
$[Nb\{(\eta\text{–}C_5H_4)C(C_5H_{10})(\eta\text{–}C_5H_4)\}(\eta^2\text{–}BH_4)]$ **(11)**	35.0 ± 1			*a*
$[V(\eta\text{–}C_5H_5)_2(\eta^2\text{–}BH_4)]$	31.8 ± 2			8
$[V\{(\eta\text{–}C_5H_4)C_2Me_4(\eta\text{–}C_5H_4)\}(\eta^2\text{–}BH_4)]$ **(12)**	41.5 ± 1	47.7	132.3	*a*

[a] This work

Table 2.9 Free energy barrier (at T_c) $\Delta G^{\ddagger}$ to bridge-terminal hydrogen exchange and bending angle β for Group 5 metallocene tetrahydroborate complexes

Substitution of BD_4 for BH_4 does not appear to affect the barrier to exchange, as evidenced by the close similarity in $\Delta G^{\ddagger}$ for the compounds **2** and **3, 16** and **17** and $[Nb\{(\eta-C_5H_4)CMe_2(\eta-C_5H_4)\}(\eta^2-BH_4)]$ and **9**.

Interestingly whereas the free energy barrier to bridge-terminal hydrogen exchange is reduced in the presence of an ethylene-bridge for the niobocene compounds, for the two-carbon bridged vanadocene compound **12** $\Delta G^{\ddagger}$ is actually increased by *ca.* 10 kJ mol^{-1} relative to the nonbridged compound $[V(\eta-C_5H_5)_2(\eta^2-BH_4)]$. However the magnitude of the change in $\Delta G^{\ddagger}$ is not as marked as for the methylene-bridged compounds. Attempts to prepare a single-carbon bridged *ansa*-vanadocene tetrahydroborate compound were unsuccessful.

2. 6 Density Functional Calculations

2.6.1 Introduction

Density functional calculations have proved very successful in reproducing changes in structure and reactivity in metallocene chemistry found on introduction of an *ansa*-bridge between the cyclopentadienyl rings.[31, 38, 39] The experimental results reported in this chapter have been examined theoretically using density functional calculations by Professor J. C. Green and N. Ashworth of this laboratory. These calculations were performed soon after the experimental results were obtained and a summary of the density functional calculations which were made and the conclusions which are drawn is presented in this section. As can be seen the calculations carried out by Professor Green and her group allow a fuller and more detailed explanation of the experimental results described in this chapter.

The molecules chosen for theoretical calculations were the nonbridged compound $[Nb(\eta-C_5H_5)_2(\eta^2-BH_4)]$ **(Ia)** and the *ansa*-bridged compounds $[Nb\{(\eta-C_5H_4)SiH_2(\eta-C_5H_4)\}(\eta^2-BH_4)]$ **(IIa)** and $[Nb\{(\eta-C_5H_4)CH_2(\eta-C_5H_4)\}(\eta^2-BH_4)]$ **(IIIa)**. **IIa** and **IIIa** differ from the compounds studied experimentally $[Nb\{(\eta-C_5H_4)SiMe_2(\eta-C_5H_4)\}(\eta^2-BH_4)]$ **(6)** and $[Nb\{(\eta-C_5H_4)CMe_2(\eta-C_5H_4)\}(\eta^2-BH_4)]$ **(IIIb)** respectively in that the methyl substituents on the bridging atom are replaced by hydrogen to save computational time. This has previously been shown not to significantly affect structure or reactivity at the metal centre.[31, 38, 39] (Note: in the theoretical calculations discussion in this chapter and **Chapter 4**, compounds not studied

experimentally in this work, or studied theoretically only, will be identified by Roman numerals i.e. **I**, **II**, **III**,….)

2.6.2 Ground State Structures

Geometry optimisations of the ground state structures of **Ia**, **IIa** and **IIIa** were carried out with the constraint of C_{2v} symmetry. Selected interatomic distances for the optimised structures are given in **Table 2.10** where they are compared with experimental values for $[Nb(\eta\text{–}C_5H_5)_2(\eta^2\text{–}BH_4)]$ **(Ib)**, **6** and **IIIb**. Agreement between the calculated and experimental values for metal carbon and metal boron distances and for the inter-ring angle α and bending angle β are good. Discrepancies between theoretical and experimental Nb-H and B-H bond distances are explicable in the light of the problem in locating hydrogen nuclei in X-ray diffraction experiments especially in the presence of a heavy atom such as niobium.

Compound	**Ia**	**Ib**	**IIa**	**6**	**IIIa**	**IIIb**
$Nb\text{-}Cp^1_{ave}$	2.35	2.36	2.36	2.365(4)	2.33	2.342(5)
$Nb\text{-}Cp^2_{ave}$	2.35	2.36	2.36	2.367(3)	2.33	2.342(5)
$Nb\text{-}H_{a,b}$	1.90	2.00	1.90	1.92(5)	1.92	1.94(7)
Nb-B	2.32	2.26	2.32	2.373	2.34	2.36(1)
$B\text{-}H_{a,b}$	1.35	1.1	1.32	1.24(5)	1.32	1.25(7)
$B\text{-}H_{c,d}$	1.21	1.1	1.21	1.11(3)	1.21	1.07(6)
α	44	50	51	53	64	66
β	136	130	129	127	116	114
$H_a\text{-}Nb\text{-}H_b$	71	56	70	62.0(20)	69	64.0(42)
$H_c\text{-}B\text{-}H_d$	110	122	110	109.6(35)	110	110.4(67)

Table 2.10 Selected calculated interatomic distances (Å) and angles (°) for the compounds $[Nb(\eta\text{–}C_5H_5)_2(\eta^2\text{–}BH_4)]$ **(Ia),** $[Nb\{(\eta\text{–}C_5H_4)SiH_2(\eta\text{–}C_5H_4)\}(\eta^2\text{–}BH_4)]$ **(IIa)** and $[Nb\{(\eta\text{–}C_5H_4)CH_2(\eta\text{–}C_5H_4)\}(\eta^2\text{–}BH_4)]$ **(IIIa)** and selected experimental interatomic distances (Å) and angles (°) for the compounds $[Nb(\eta\text{–}C_5H_5)_2(\eta^2\text{–}BH_4)]$ **(Ib),** $[Nb\{(\eta\text{–}C_5H_4)SiMe_2(\eta\text{–}C_5H_4)\}(\eta^2\text{–}BH_4)]$ **(6)** and $[Nb\{(\eta\text{–}C_5H_4)CMe_2(\eta\text{–}C_5H_4)\}(\eta^2\text{–}BH_4)]$ **(IIIb)**

2.6.3 Mechanism for Bridge-Terminal Hydrogen Exchange

A possible mechanism for bridge-terminal hydrogen exchange is shown in **Figure 2.16.** At the mid-point of the exchange reaction the interchanging hydrogens must be in equivalent positions. This is ensured in the proposed pathway by the presence of xz as a mirror plane. Thus H_a stays in the same position in the exchange process. The energy difference between the ground and transition states for the three compounds **Ia**, **IIa** and **IIIa** are given in **Table 2.11**. Agreement with the experimental values of $\Delta G^{\ddagger}$ is good making this an excellent candidate for the exchange process. The Nb-H and B-H distances in the transition states are also given in **Table 2.11**. These suggest that whereas H_a remains strongly bound to the metal, H_b and H_c are only weakly bound. Whether the binding in the transition state is described as η^1 or η^3 (**Section 2.2**) is a matter of semantics. However it should be noted that both these nomenclatures imply a local C_3 axis for the $[NbBH_4]$ unit and the proposed transition state clearly lacks this.

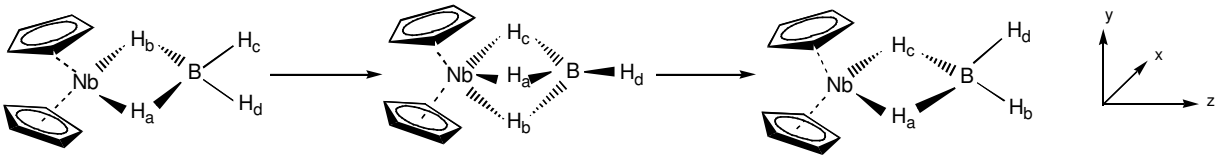

Figure 2.16 Proposed mechanism for bridge-terminal hydrogen exchange in niobocene tetrahydroborate complexes

Property	**Ia**	**IIa**	**IIIa**
Calculated energy above ground state	64.1	52.1	35.4
Experimental $\Delta G^{\ddagger}$	61.0	49.3	35.0
Nb-H_a	1.931	1.935	1.956
Nb-$H_{b,c}$	2.258	2.204	2.176
B-H_a	1.328	1.328	1.319
B-$H_{b,c}$	1.227	1.230	1.236
B-H_d	1.204	1.202	1.202

Table 2.11 Energies (kJ mol^{-1}) and selected distances (Å) for proposed transition state

2.6.4 Bonding Considerations

A metallocene fragment presents three frontier orbitals for binding in the xz plane, $4a_1$, $2b_1$ and $3a_1$ (**Section 1.1.2**). **Figure 2.17** shows a MO diagram for the ground state structure of the compound **Ia**, constructed from [Nb(η−$C_5H_5)_2$] and [BH_4] fragments. The HOMO of a_1 symmetry is d_x^2 in character. Below this lie four orbitals with their principal origin in the bent metallocene fragment, being largely cyclopentadienyl in character. These are followed by three orbitals of mainly B-H origin. The highest of the three is of b_2 symmetry, largely localised on the the terminal hydrogens and is not involved in $NbBH_4$ binding. The lower pair have a_1 and b_1 symmetry and some metal character; these are the orbitals which bind the BH_4 unit to the metallocene. The interactions are depicted in **Figure 2.18**.

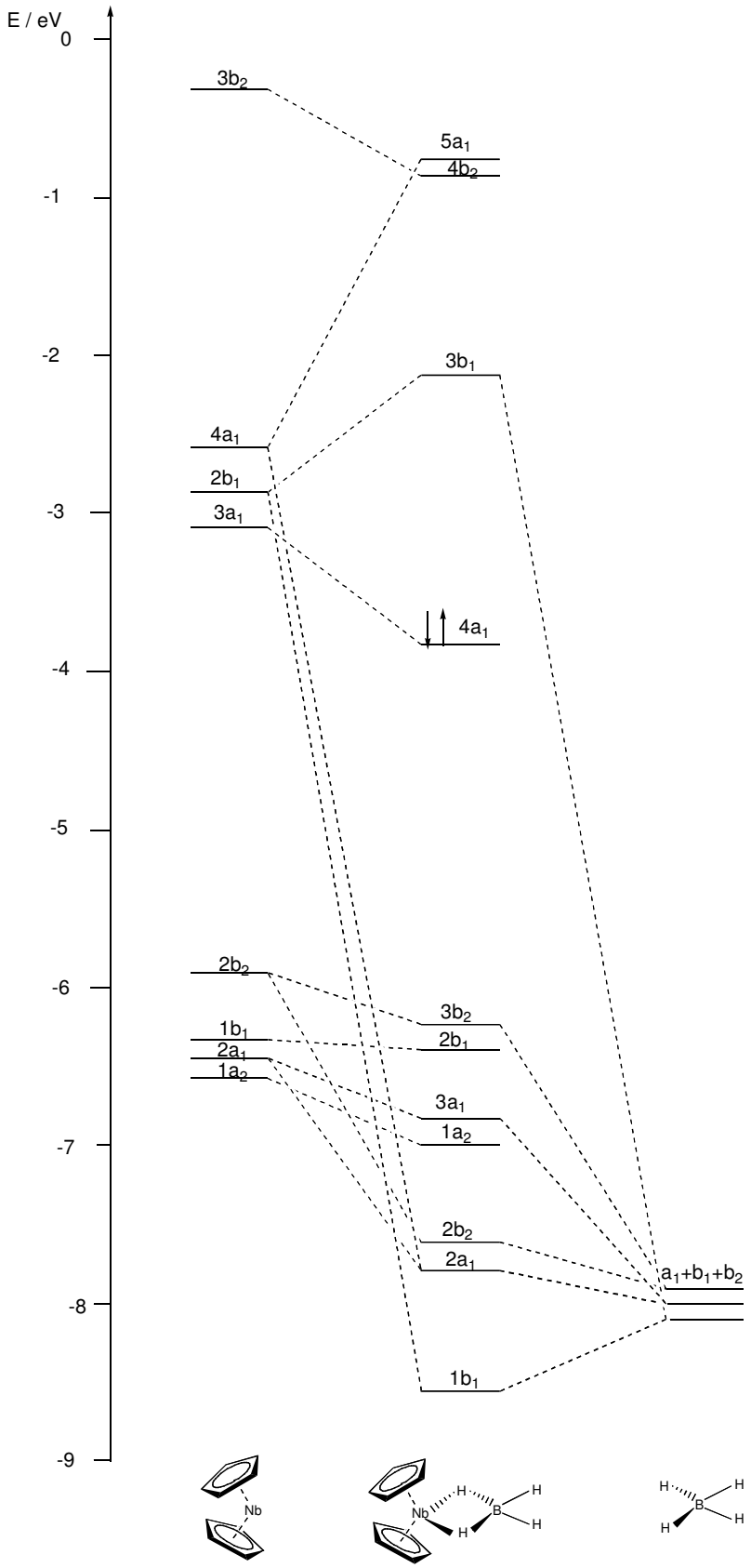

Figure 2.17 MO scheme for $[Nb(\eta\text{–}C_5H_5)_2(\eta^2\text{–}BH_4)]$

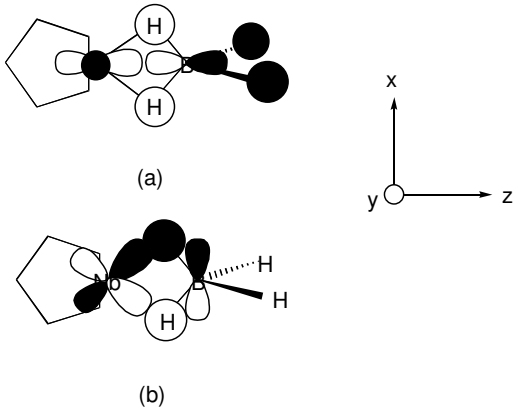

Figure 2.18 Representations of bonding interactions in $[Nb(\eta\text{–}C_5H_5)_2(\eta^2\text{–}BH_4)]$
(a) Nb-BH_4 a_1 ground state interaction (b) Nb-BH_4 b_1 ground state interaction

Population analyses of the metallocene and borohydride frontier orbitals of **Ia**, **IIa** and **IIIa** enables a comparison of bonding in the ground state structures to be made. Gross populations of the metallocene $3a_1$, $2b_1$, $4a_1$ and $3b_2$ orbitals and the BH_4 $2a_1$, $1b_1$ and $1b_2$ orbitals are given in **Table 2.12**. In a metallocene cation $3a_1$ would have an occupancy of 2 while $4a_1$ and $2b_1$ would have an occupancy of 0. All three BH_4 frontier orbitals in a tetrahydroborate anion would have an occupancy of 2. Thus the degree of departure from occupancies of either 2 or 0 give the amount of covalent mixing between the metallocene and tetrahydroborate orbitals. For all three compounds there is more mixing in b_1 than a_1 consistent with the $4a_1$ orbital of the metallocene fragment being higher in energy than the $2b_1$. The degree of mixing in a_1 decreases sharply with increasing inter-ring angle α and decreasing bending angle β from **Ia** to **IIa** to **IIIa.** As described in **Section 1.1.2** the $4a_1$ orbital rises steeply in energy with increasing inter-ring angle. The b_1 interaction also decreases with increased bending of the rings as the *ansa*-bridge constrains the metallocene geometry, although the effect is not as marked as for a_1. The weaker metal-borohydride interactions for the carbon bridged compound **IIIa** are consistent with the longer Nb-$H_{a,b}$ and Nb---B distances calculated (**Table 2.10**) and the trends in B-H stretching frequencies discussed in **Section 2.5.2**. Thus as the inter-ring angle α is increased and the bending angle β decreased in the ground state structure, the BH_4 unit becomes more weakly bound.

	Ia gs	**IIa** gs	**IIIa** gs	**Ia** ts	**IIa** ts	**IIIa** ts
$[Nb(\eta-C_5H_5)_2]$						
$3b_2$	0.03	0.03	0.05	0.12	0.14	0.17
$4a_1$	0.36	0.24	0.18	0.22	0.16	0.12
$2b_1$	0.36	0.35	0.31	0.32	0.32	0.30
$3a_1$	1.83	1.86	1.89	1.86	1.86	1.88
$[BH_4]$						
$2a_1$	1.71	1.78	1.82	1.81	1.82	1.85
$1b_1$	1.65	1.67	1.71	1.70	1.72	1.72
$1b_2$	1.92	1.91	1.89	1.85	1.84	1.81

Table 2.12 Gross occupancies of $[Nb(\eta-C_5H_5)_2]$ and $[BH_4]$ frontier orbitals in **Ia**, **IIa** and **IIIa** in their η^2 ground state (gs) and in the proposed transition state (ts)

A comparison is also possible between the bonding in the proposed transition states. The structure is such that the exchanging hydrogens H_b and H_c lie above and below the xz plane and approach the metal sufficiently to interact with the metal dyz orbital (**Figure 2.19**). This may be envisaged as donation from BH_4 into the high lying $3b_2$ orbital, not normally considered as a frontier orbital in a metallocene. The $3b_2$ orbital has its parentage in one of the antibonding e_1" orbitals of the parallel metallocene and this metal-ring antibonding nature is also depicted in **Figure 2.19**. As the bending of the metallocene is increased this $3b_2$ orbital drops in energy. Thus this orbital is expected to be most available to the carbon-bridged compound **IIIa** which has the largest value of α for the series. Inspection of the gross occupancies of the metallocene $3b_2$ orbital and BH_4 $1b_2$ orbital in the transition state structures in **Table 2.12** confirm that the degree of mixing between the b_2 orbitals is greatest in this case. It is also the case that the carbon-bridged compound **IIIa**, having the lowest a_1 and b_1 occupancies in the ground state structures, suffers less loss of this mixing on going to the transition state relative to the silicon-bridged and nonbridged compounds **IIa** and **Ia** respectively. Thus as the introduction of an *ansa*-bridge increases the bending of the rings, as evidenced by increasing α and decreasing β, the BH_4 unit becomes more weakly bound in the ground

state and the transition becomes more accessible, lowering the energy barrier to bridge-terminal hydrogen exchange.

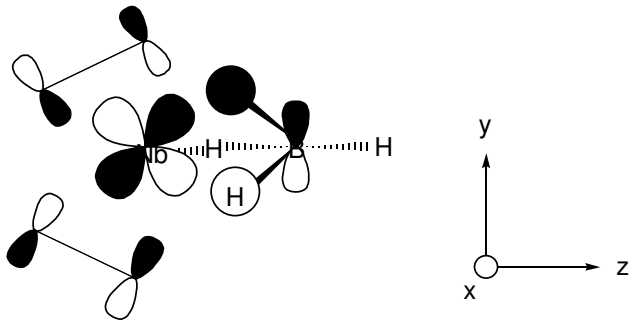

Figure 2.19 Representation of Nb-BH_4 transition state bonding interactions in $[Nb(\eta\text{–}C_5H_5)_2(\eta^2\text{–}BH_4)]$

2.7 Summary

This chapter describes the structural and dynamic properties of Group 5 *ansa*-metallocene tetrahydroborate complexes. The new chemistry reported is summarised in **Scheme 2.18**. Variable temperature ^1H NMR spectroscopy has allowed the elucidation of the free energy barrier $\Delta G^{\ddagger}$ to bridge-terminal hydrogen exchange in the tetrahydroborate ligand. $\Delta G^{\ddagger}$ is considerably reduced when the bridging unit imposes significant structural changes in the metallocene.[40] Density functional calculations have identified a transition state for the exchange process.[41] As the inter-ring angle α is increased and the ring bending angle β reduced upon the introduction of an *ansa*-bridge, the M-BH_4 covalent interaction decreases whereas binding of the tetrahydroborate unit increases in the transition state. Both effects contribute to the lowering of the energy barrier.

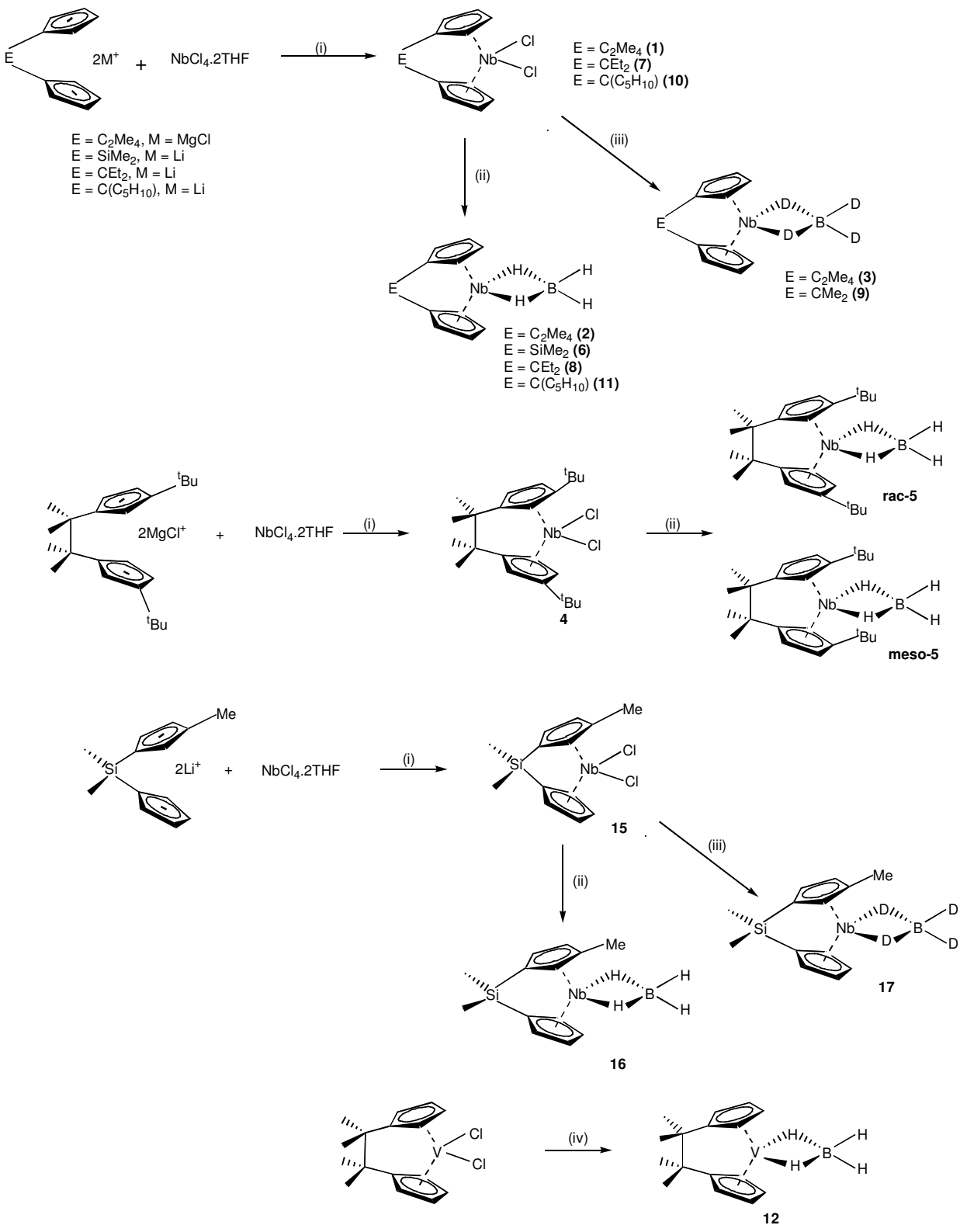

Conditions (i) Diethyl ether. (ii) $LiBH_4$ in DME. (iii) $NaBD_4$ in DME.

(iv) $NaBH_4$ in DME.

Scheme 2.18 New chemistry presented in Chapter 2

2.8 References

1 T. J. Marks and J. R. Kolb, *Chem. Rev.*, 1977, **77**, 263.
2 F. Tagusagawa, A. Fumagalli, T. F. Koetzle, S. G. Shore, T. Schmitkons, A. V. Fratini, K. W. Morse, C. Y. Wei and R. Bau, *J. Am. Chem. Soc.*, 1981, **103**, 5165.
3 R. Bau, H. S. Yuan, M. V. Baker and L. D. Field, *Inorg. Chim. Acta*, 1986, **114**, L27.
4 J. A. Jensen and G. S. Girolami, *J. Am. Chem. Soc.*, 1988, **110**, 4450.
5 A. Almenningen, G. Gundersen and A. Haaland, *Acta Chem. Scand.*, 1968, **22**, 328.
6 I. Chuang, T. J. Marks, W. J. Kennedy and J. R. Kolb, *J. Am. Chem. Soc.*, 1977, **99**, 7539.
7 K. M. Melmed, D. Coucouvanis and S. J. Lippard, *Inorg. Chem.*, 1972, **12**, 232.
8 T. J. Marks and W. J. Kennelly, *J. Am. Chem. Soc.*, 1975, **97**, 1439.
9 C. R. Lucas and M. L. H. Green, *J. Chem. Soc., Chem. Commun.*, 1972, 1005.
10 N. J. Bailey, M. L. H. Green, M. A. Leech, J. F. Saunders and H. M. Tidswell, *J. Organomet. Chem.*, 1997, **538**, 111.
11 P. L. Johnson, S. A. Cohen, T. J. Marks and J. M. Williams, *J. Am. Chem. Soc*, 1978, **100**, 2709.
12 T. J. Marks and L. A. Shrimp, *J. Am. Chem. Soc.*, 1982, **94**, 1542.
13 M. L. H. Green and L. L. Wong, *J. Chem. Soc., Dalton Trans.*, 1989, 2133.
14 B. Dorer, J. Diebold, O. Weyand and H. H. Brintzinger, *J. Organomet. Chem.*, 1992, **427**, 245.
15 B. Dorer, M. H. Prosenc, U. Rief and H. H. Brintzinger, *Organometallics*, 1994, **13**, 3868.
16 B. Dorer, M. -H. Prosenc, U. Rief and H. H. Brintzinger, *Collection of Czechoslovak Chemical Communications*, 1997, **62**, 265.
17 M. E. Huttenloch, B. Dorer, U. Rief, M. H. Prosenc, K. Schmidt and H. H. Brintzinger, *J. Organomet. Chem.*, 1997, **541**, 219.
18 N. J. Bailey, J. A. Cooper, H. Gailus, M. L. H. Green, J. T. James and M. A. Leech, *J. Chem. Soc., Dalton Trans.*, 1997, 3579.
19 W. A. Herrmann, W. Baratta and E. Herdtweck, *J. Organomet. Chem.*, 1997, **541**, 445.
20 A. Antiñolo, M. Martinez-Ripoll, Y. Mugnier, A. Otero, S. Prashar and A. M. Rodriguez, *Organometallics*, 1996, **15**, 3241.
21 L. Labella, A. Chernega and M. L. H. Green, *J. Organomet. Chem.*, 1995, **485**, C18.
22 A. Chernega, J. Cook, M. L. H. Green, L. Labella, S. J. Simpson, J. Souter and A. H. H. Stephens, *J. Chem. Soc., Dalton Trans.*, 1997, 3225.
23 S. L. J. Conway, T. Dijkstra, L. H. Doerrer, J. C. Green, M. L. H. Green and A. H. H. Stephens, *J. Chem. Soc., Dalton Trans.*, 1998, 2689.
24 H. Schwemlein and H. H. Brintzinger, *J. Organomet. Chem.*, 1983, **254**, 63.
25 R. L. Benoit and S. Y. Lam, *J. Am. Chem. Soc.*, 1974, **24**, 7385.
26 R. A. Bell, S. A. Cohen, N. M. Doherty, R. S. Threlkel and J. E. Bercaw, *Organometallics*, 1986, **5**, 972.
27 N. I. Kurillova, A. I. Gusev and Y. T. Struchkov, *Zh. Strukt. Khim.*, 1974, **15**, 718.
28 R. M. Shaltout, J. Y. Corey and N. P. Rath, *J. Organomet. Chem.*, 1995, **503**, 205.
29 M. J. Drewitt, S. Barlow, D. O'Hare, J. M. Nelson, P. Nguyen and I. Manners, *J. Chem. Soc., Chem. Commun.*, 1996, 2153.
30 C. S. Bajgur, W. R. Tikkanen and J. L. Petersen, *Inorg. Chem.*, 1985, **24**, 2539.

31 J. C. Green and A. Scottow, *N. J. Chem.*, 1999, **23**, 651.
32 J. A. Ewen, *J. Am. Chem. Soc.*, 1984, **106**, 6355.
33 M. L. H. Green and N. Ishihara, *J. Chem. Soc., Dalton Trans.*, 1994, 657.
34 H. G. Alt and R. Zenk, *J. Organomet. Chem.*, 1996, **526**, 295.
35 D. R. Lantero, D. L. Ward and M. R. Smith III, *J. Am. Chem. Soc.*, 1997, **119**, 9699.
36 J. A. Jensen and G. S. Girolami, *Inorg. Chem.*, 1989, **28**, 2107.
37 J. C. Green, *Chem. Soc. Rev.*, 1998, 263.
38 J. C. Green and C. N. Jardine, *J. Chem. Soc., Dalton Trans.*, 1998, 1057.
39 S. L. J. Conway, L. H. Doerrer, J. C. Green, M. L. H. Green, A. Scottow and A. H. H. Stephens, *J. Chem. Soc., Dalton Trans.*, 2000, 329
40 S. L. J. Conway, L. H. Doerrer, M. L. H. Green and M. A. Leech, *Organometallics*, 2000, **19**, 630.
41 N. Ashworth, S. L. J. Conway, J. C. Green and M. L. H. Green, Submitted for publication.